Toroidal modeling of runaway electron loss due to 3-D fields in ITER

Yueqiang Liu[1], K. Aleynikova[2], C. Paz-Soldan[3], P. Aleynikov[2], V. Lukash[4], R. Khayrutdinov[4]

[1]General Atomics, PO Box 85608, San Diego, CA 92186-5608, USA
[2]Max-Planck-Institut fur Plasmaphysik, Teilinsitut Greifswald, D-17491 Greifswald, Germany
[3]Department of Applied Physics and Applied Mathematics, Columbia University, New York, NY 10024, USA
[4]National Research Center Kurchatov Institute, Moscow, Russia

E-mail: liuy@fusion.gat.com

Abstract. Mitigation of runaway electrons (REs) by three-dimensional (3-D) magnetic field perturbations is numerically investigated for the ITER 15 MA baseline D-T scenario, utilizing the MARS-F code [Liu *et al* Phys. Plasmas **7** 3681] with a drift orbit test particle tracing module. Considered are two types of 3-D fields: the $n = 3$ (n is the toroidal mode number) resonant magnetic perturbation (RMP) utilized for the purpose of controlling the edge localized modes in ITER, and perturbations generated by the $n = 1$ magneto-hydrodynamic (MHD) instabilities in a post-disruption plasma. The RMP field, applied to a pre-disruption plasma, is found to be moderately effective in mitigating the RE seeds in ITER when vacuum field model is assumed. Up to $\sim$40% loss fraction is possible at 90 kA-turn coil current. The mitigation efficiency is however substantially reduced, down to less than 5%, when the plasma response is taken into account. This is due to strong screening of the resonant magnetic field components by the plasma response resulting in much less field line stochasticity. On the other hand, the MARS-F modeling, based on the DINA-simulated post-disruption equilibria, shows that the $n = 1$ resistive kink instabilities develop in these plasmas, as the edge safety factor q_a evolves and drops below integer numbers. RE mitigation by these MHD instabilities is sensitive to the eigenmode structure. The best mitigation is achieved as q_a drops below 3, when a global kink instability occurs that encompasses both internal and external components. This global instability is found to be capable of mitigating over 80% MeV-level passing RE orbits at a field perturbation $|\delta B|/B_0$ that is comparable to that observed in DIII-D experiments, and full mitigation if the perturbation amplitude is doubled. The "wetted" area on the ITER limiting surface, due to MHD instability induced RE loss, generally increases with the perturbation amplitude (together with increasing loss fraction). At the highest perturbation level assumed in this study, the wetted area reaches $\sim$60% of the total limiting surface area. The lost RE orbits mainly strike the outer divertor region of the limiting surface, with some fraction also hitting a wide area along the inboard side of the surface.

Keywords: runaway current, 3-D field, RE loss

1. Introduction

The presence of high-energy, relativistic runaway electrons (RE) is one of the significant concerns, along with the thermal and mechanical loads, if plasma disruptions occur in ITER high-current plasmas [1]. The fundamental reason for large RE current is that, once the RE seeds are generated, an avalanche process can be triggered that leads to exponential growth of the runaway current [2]. Crucially, the e-folds number during avalanche is proportional to the pre-disruption plasma current. For ITER with 15 MA plasma current operation, this leads to formation of a potentially huge runaway current, up to 10 MA [3], which may pose severe issue on the integrity of the plasma facing components (PFCs). In fact, even in present-day devices such as JET, melting of the metal surface was observed due to localized strikes of REs on the plasma facing components [4]. Investigating various possible techniques for RE mitigation is therefore an urgent task for the ITER operation.

The RE physics dictates two possible ways to control the runaway current. One is to prevent the primary seed generation. The other, less attractive approach, is to purge well-established RE beam after the avalanche amplification, if the seed prevention turns out to be challenging. Both ways need to be carefully exploited to ensure safe operation of ITER. A typical way of solving the RE seeding issue is to increase the electric field threshold needed for seed generation [5], by increasing the electron density [6]. This technique, however, may not be effective for other seed generation mechanisms such as the hot-tail formation which is primarily due to fast thermal quench [7] or tritium decay [8]. Another way to control RE seeding is to apply three-dimensional (3-D) magnetic field perturbations. Experiments in ASDEX Upgrade showed encouraging results with this approach [9], where the applied field perturbation modifies the electron temperature which in turn may affect the hot-tail formation. 3D magnetic fields, either due to turbulence [10], intentionally applied resonant magnetic perturbations (RMPs) [11–13], or naturally occurring due to magneto-hydrodynamic (MHD) instabilities [14, 15, 20], have also been shown to be useful for controlling well-established RE beams. We mention that other RE mitigation techniques have also been extensively investigated in experiments [16–19, 21] and theory [22–25] during recent years.

This work focuses on direct modeling of the RE mitigation due to 3-D fields for the ITER 15 MA baseline scenario. For this purpose, we consider two types of fields. One is the RMP generated by magnetic coils designed for controlling the edge localized modes (ELMs) in ITER. The primary objective here is to find out whether the RMP field is effective in de-confining RE seeds. Compared to the previous study for ITER [11], we take into account the plasma response to the applied RMP, which, as we will show in this study, plays a significant role in RE loss. The other type of the field is passively generated by the occurrence of MHD instabilities in post-disruption ITER equilibria simulated by the DINA code [26, 27]. Such macroscopic instabilities, when grow to large

magnitudes, have been found to be effective in mitigating runaway beams in DIII-D experiments [15]. We will show that similar MHD instabilities are indeed predicted to occur in ITER post-disruption plasmas as well, and this leads to substantial RE mitigation.

For the RE loss study in ITER, it is important to not only quantify the loss fraction but also to understand where the lost REs strike the plasma facing components. A strike that is too localized is certainly undesirable, in particular given the MA-level post-disruption runaway current that is expected to be generated due to the avalanche effect in ITER. In other words, we wish to have a large "wetted area" due to lost REs hitting the plasma facing components. This is another important aspect that we investigate in this work. The 2-D ITER limiting surface is considered here, which is the closest surface facing the plasma. Future work may consider the fully 3-D PFC configuration.

It is important to note that we do not directly model the RE seed generation or the avalanche processes in this work. Instead, we assume a given initial RE distribution, and trace the particle drift orbit trajectories in the presence of 3-D fields. The emphasis here is to consider accurate toroidal models for the perturbed field structure in ITER plasmas. These 3-D fields are computed by the MARS-F code [28] in this study.

The paper is structured as follows. Section 2 briefly describes the simulation models. Section 3 reports the RE loss modeling due to the RMP field in ITER. The main results are presented in Section 4, where the possibility of MHD instability-facilitated RE beam mitigation is investigated for ITER. Section 5 summarizes the work.

2. Toroidal formulation for RE loss modeling

In this work, we utilize the linear, resistive MHD code MARS-F [28] to compute the 3-D fields in ITER, either due to RMP (including the plasma response) or due to the MHD instabilities. The code solves single fluid, full MHD equations in toroidal geometry. An equilibrium magnetic flux-based curvilinear coordinate system is used in MARS-F. It is important to note that the RE tracing is carried out in the same coordinates, ensuring high-fidelity representation of the 3-D perturbations when the RE orbits are modeled. Detailed formulation for computing the plasma response to RMP is described in Ref. [29]. Below, we show the perturbed MHD equations that MARS-F solves for the resistive stability problem, that is relevant to the main results of this study

$$\gamma\xi = \mathbf{v}, \tag{1}$$

$$\rho\gamma\mathbf{v} = -\nabla p + \mathbf{j}\times\mathbf{B} + \mathbf{J}\times\delta\mathbf{B}, \tag{2}$$

$$\gamma\delta\mathbf{B} = -\nabla\times\delta\mathbf{E}, \tag{3}$$

$$\delta\mathbf{E} = -\mathbf{v}\times\mathbf{B} + \eta\mathbf{j}, \tag{4}$$

$$\gamma\delta p = -\mathbf{v}\cdot\nabla P - \Gamma P\nabla\cdot\mathbf{v}, \tag{5}$$

$$\mathbf{j} = \nabla\times\delta\mathbf{B}, \tag{6}$$

where $\rho, \mathbf{B}, \mathbf{J} = \nabla\times\mathbf{B}, P$ denote the equilibrium plasma density, magnetic field, the plasma current density, and the plasma pressure, respectively. The quantities

$\xi, \mathbf{v}, \delta\mathbf{B}, \delta\mathbf{E}, \mathbf{j}, \delta p$, are the solution variables representing the plasma displacement, the perturbed fluid velocity, magnetic and electric fields, plasma current and pressure, respectively. In the single fluid MHD approximation, the ratio of specific heats, Γ from Eq. (5), is taken to be 5/3 as for an ideal gas. η is the plasma resistivity.

We emphasize one aspect here on the plasma resistivity, which plays a central role in both the plasma response and the MHD instability computations in this work. The Spitzer resistivity model is implemented in the code. For ITER, this means that the plasma resistivity is very low in a pre-disruption plasma, leading to nearly ideal plasma response (thus significant screening of the resonant components) of the applied RMP field. On the other hand, the plasma resistivity is much higher in a post-thermal quench plasma, leading to resistive MHD instabilities that behave as ordinary ideal kink instabilities with fast growth rate (although the ideal counterpart is stable for some of the equilibria considered in this work). This is important for generating perturbations with large amplitude in post-disruption plasmas, which then facilitate RE purging.

The RE loss study is carried out by tracing guiding center drift orbits of test particles in a given field perturbation computed by MARS-F. A RE orbit (REORBIT) module has been developed for this purpose [20, 30], which is relevant for tracing relativistic particles. As mentioned earlier, the RE orbit is time-advanced in the flux-based curvilinear coordinate system (s, χ, ϕ), where $s \equiv \sqrt{\psi_p}$ (ψ_p is the equilibrium poloidal flux normalized to 0 at the magnetic axis and 1 at the plasma boundary surface) labels the plasma radial coordinate, χ is a generic poloidal angle and ϕ the geometric toroidal angle

$$\frac{ds}{dt} = \mathbf{v}_{gc} \cdot \nabla s, \tag{7}$$

$$\frac{d\chi}{dt} = \mathbf{v}_{gc} \cdot \nabla \chi, \tag{8}$$

$$\frac{d\phi}{dt} = \mathbf{v}_{gc} \cdot \nabla \phi, \tag{9}$$

where $\mathbf{v}_{gc}$ is the particle guiding center velocity taking into account the relativistic effect [20]

$$\mathbf{v}_{gc} = \frac{1}{-e\hat{\mathbf{b}} \cdot \mathbf{B}^*} \hat{\mathbf{b}} \times \left(e\mathbf{E}^* + \frac{m_e c^2}{\gamma_g B_0} M \nabla B_{\rm tot} + \frac{m_e c^2}{\gamma_g} p_\parallel^2 \kappa \right) + v_\parallel \hat{\mathbf{b}}, \tag{10}$$

with e being the charge unit, $\hat{\mathbf{b}} \equiv \mathbf{B}_{\rm tot}/B_{\rm tot}, \mathbf{B}_{\rm tot} = \mathbf{B} + \delta\mathbf{B}, B_{\rm tot} = |\mathbf{B}_{\rm tot}|$, m_e the electron mass at rest, c the speed of light, γ_g the Lorentz factor, B_0=5.3 T the vacuum toroidal field at the major radius of R_0=6.2 m in ITER, $M \equiv p_\perp^2/(2b)$ the (normalized) particle magnetic moment with $b = B_{\rm tot}/B_0$, and κ the magnetic curvature of the total field $\mathbf{B}_{\rm tot}$. $v_{||}$ is the particle parallel velocity along the perturbed magnetic field lines. $p_\perp$ and $p_{||}$ represent the perpendicular and parallel components of the electron momentum $\mathbf{P} = \gamma_g m_e \mathbf{v}_{gc}$ normalized by $m_e c$. $\mathbf{B}^*$ and $\mathbf{E}^*$ are the total magnetic and electric fields, respectively, including the relativistic corrections

$$\mathbf{B}^* = \mathbf{B}_{\rm tot} - \frac{P_\parallel}{eB_{\rm tot}} \nabla \times \mathbf{B}_{\rm tot}, \tag{11}$$

$$\mathbf{E}^* = \mathbf{E}_{\rm tot} - \frac{P_\parallel}{eB}_{\rm tot} \nabla \times \mathbf{E}_{\rm tot}, \tag{12}$$

where $\mathbf{E}_{\rm tot} = \mathbf{E}_{\rm eq} + \delta\mathbf{E}$ and $\mathbf{E}_{\rm eq} = \eta\mathbf{J}$.

The normalized electron momentum p and the particle velocity pitch angle $\lambda \equiv v_\perp^2/(v_{gc}^2 b)$ are also time integrated according to

$$\tau_c \frac{dp}{dt} = \mu E - \left(1 + \frac{1}{p^2}\right) - \frac{\lambda p \gamma b}{\tau} - F_B, \tag{13}$$

$$\tau_c \frac{d\lambda}{dt} = -\frac{2\mu\lambda E}{p} + \frac{2\mu^2\gamma}{bp^3}(1+Z) - \frac{2\lambda\mu^2}{\tau\gamma} - 2\mu\sqrt{\frac{\lambda\gamma}{bp^3}(1+Z)}\frac{dW_t}{dt}, \tag{14}$$

where the relativistic collision time scale is $\tau_c = m_e c/eE_c$, with $E_c = n_e e^3 \ln\Lambda/(4\pi\epsilon_0^2 m_e c^2)$ and n_e being the thermal electron density, $\ln\Lambda$ the Coulomb logarithm, and ϵ_0 the vacuum permittivity. $\mu = p_\parallel/p$, and E is the parallel component of the total electric field $\mathbf{E}_{\rm tot}$ normalized by $-E_c$. The factor τ in the above equations is defined as $\tau = \tau_r/\tau_c$, with $\tau_r = 6\pi\epsilon_0 m_e^3 c^3/(e^4 B_0^2)$ defining the synchrotron radiation time scale. Z is the nucleus charge number of the impurity species.

The first terms from the right hand side of the RE velocity Eqs. (13) and (14) represent the parallel electric field acceleration/deceleration. The second terms are due to small angle collision, including that with impurity nucleus which modifies the particle pitch angle but conserves the particle energy. The third terms, associated with the τ factor, are due to synchrotron radiation. The last term from Eqs. (13) represents the Bremsstrahlung drag [20] and the last term from Eq. (14) represents the Wiener process W_t, with increments drawn from Gaussian distribution with zero mean and variance equal to dt [31]. Conceptually, W_t represents a random walk process.

Equations (7)-(9) and (13)-(14) are time-advanced with initial conditions $\psi_p = s_0^2, \chi = \chi_0, \phi_0, p = p_0, \lambda = \lambda_0$ and $\sigma = \sigma_0$ at $t = 0$. Here, σ_0 specifies the initial direction of the RE parallel velocity, with $\sigma_0 = +1$ defined as the direction parallel to the equilibrium plasma current (co-current), and $\sigma_0 = -1$ in the counter-current direction. An adaptive time advance solver LSODE [32] is adopted to ensure numerical accuracy and efficiency of the RE orbit tracing. All REs are launched from inside the plasma and the drift orbit tracing is terminated after an upper bound of the simulation time is reached, or if the particle hits the limiting surface.

3. RE loss due to RMP fields

In what follows, we investigate the possibility of RE de-confinement by RMP fields for an ITER plasma. The motivation here is two-fold. First, it is interesting to examine whether the RMP field, produced by the ELM control coils designed for ITER, can be effective in mitigating REs. Previous modeling work shows minor effect of RMP on RE loss in DIII-D [30]. On the other hand, both experiments [13] and modeling [30] in COMPASS have shown certain efficiency of RMP fields on directly mitigating the runaway current in post-disruption COMPASS plasmas. The question is whether a

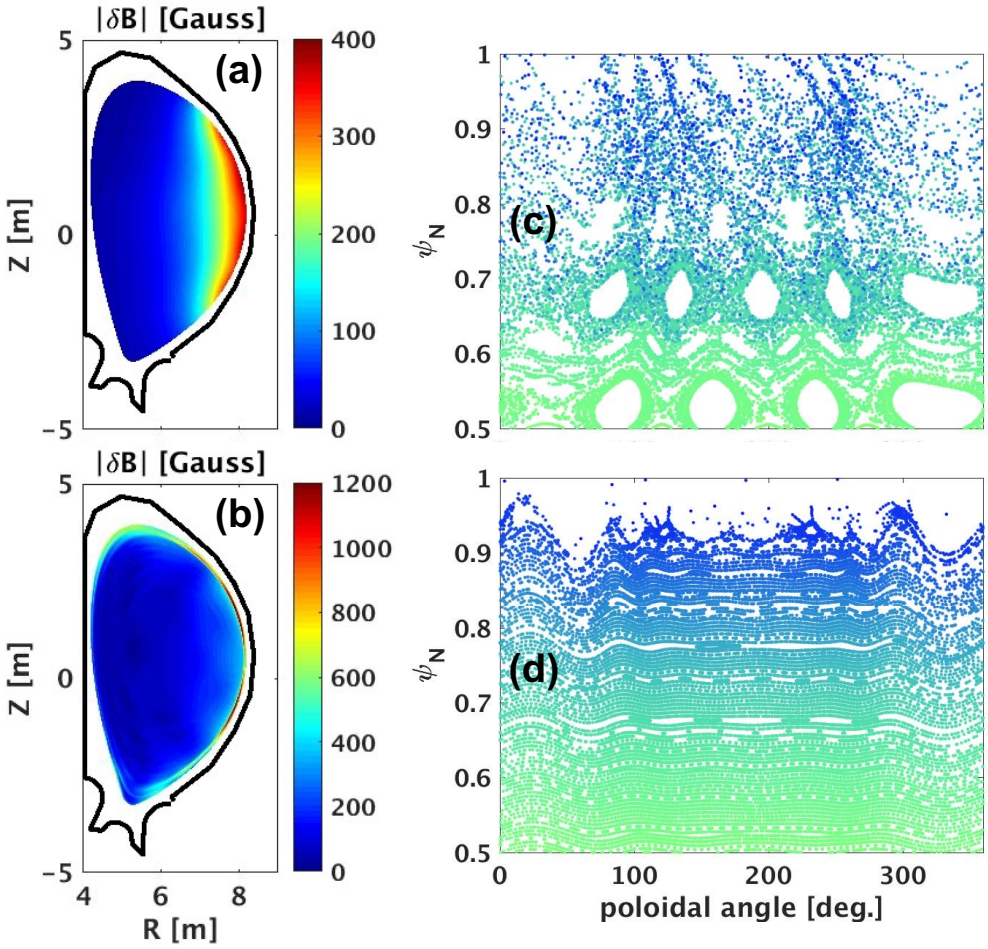

Figure 1. Comparison of the 3-D magnetic field perturbation inside the ITER plasma, in terms of the (a-b) the perturbed field amplitude and (c-d) the Poincaré plots of the field line tracing, between (a,c) the vacuum field and (b,d) the total perturbation including the plasma response. The solid lines in (a-b) show the ITER limiting surface. The vacuum field is produced by three rows of the ELM control coils at 90 kA-turn (kAt) coil current, with the $n = 3$ waveform and the coil phasing of (200°, 0°, 140°) for the upper, middle and lower rows, respectively. Considered is an ITER 15 MA pre-disruption plasma from the $Q = 10$ baseline D-T scenario.

similar effect can be achieved in ITER. We mention that RE de-confinement by RMP has previously been modeled for ITER [11], showing rapid loss of REs located in the region with the normalized toroidal flux larger than 0.5. Vacuum RMP field approximation was adopted in Ref. [11]. As will be shown in this study, taking into account the plasma response can substantially modify the field perturbation structure and hence change the prediction for the RE loss in ITER. Furthermore, the present work carries out RE loss study in the context of the ELM control coil configuration expected to be used in ITER, by assuming optimized coil phasing among three rows of the magnetic coils [33]. This was not considered in Ref. [11].

Another, perhaps more important, motivation is to examine whether it is possible

to utilize the RMP field to influence the RE seeding in ITER. Given the potentially severe consequence of a well-formed, large RE current (after avalanche) on the ITER wall (even if mitigated by MHD instabilities to be also shown in this work), it is certainly desirable to have possibilities of eliminating REs before or during the initial phase of disruption. Experimental results in ASDEX Upgrade [9] and recent modeling efforts [34] have demonstrated that this is a promising approach. For this reason, we will consider a pre-disruption reference ITER equilibrium from the fusion power operation (D-T) phase, i.e. a plasma from the 15 MA baseline scenario. We note that such a plasma still has too high thermal electron temperature to allow efficient hot-tail generation of RE seeds. Therefore, the initial RE distribution that we assume here is of *ad-hoc* nature. Our main purpose here is to model how the RMP field can de-confine REs, with less consideration on how these RE seeds are actually generated. The lower energy RE seeds due to tritium decay (which we also model here) are of course less sensitive to the assumed equilibrium.

It should also be noted that the ELM control coils are much closer to the plasma during the pre-disruption phase, resulting in much larger RMP field inside the plasma (with the same coil current) than the case of a post-disruption plasma with a well-formed RE beam, which is typically located far from the ELM control coils due to the plasma shrinkage and vertical shift during disruption (as will be shown later on in this study). The narrower plasma-coil gap is one of the reasons that RMP is more efficient for RE mitigation in COMPASS than in DIII-D [30].

For the chosen plasma scenario (15 MA plasma current, 5.3 T toroidal field and fusion gain factor of $Q = 10$), the ELM control coil current optimization has previously been performed including the plasma response [33]. A coil phasing, that maximizes the resonant response in the plasma edge region for the $n = 3$ perturbation, has been identified as $(200^o, 0^o, 140^o)$ for the upper, middle and lower rows of the ELM control coils in ITER. This is the coil current configuration that yields the maximum plasma resonant field amplification and best facilitates ELM control, according to the semi-empirical criteria established in Refs. [38, 39]. In subsection 3.1, we will investigate the RE loss properties assuming the above optimal coil current configuration. An opposite case, with the coil phasing that minimizes the plasma edge resonant response, will be reported in subsection 3.2.

Figure 1 compares the field perturbation structure inside the plasma, between the vacuum field approximation and that including the plasma response. We assume 90 kA-turn (kAt) coil current which is the maximum level designed in ITER, and the aforementioned coil phasing of $(200^o, 0^o, 140^o)$. It is evident, comparing the perturbed field amplitude (Fig. 1(a-b)), that a strong field amplification occurs due to the plasma response, near the plasma edge as compared to the vacuum field. The peak value of $|\delta B|$, over the plasma volume, is increased by a factor of ~ 3 with inclusion of the plasma response. On the other hand, the resonant radial field perturbation is significantly shielded by the plasma, as shown by the Poincaré plots of the field line tracing (Fig. 1(c-d)). Here, the radial coordinate is labelled by the normalized

equilibrium poloidal flux $\psi_N = \psi_p$, that is equal to 0 on the magnetic axis and unity at the plasma boundary. The poloidal angle is defined in terms of the equal arc-length along the poloidal circumference. The large magnetic islands, that are present with the vacuum field approximation (Fig. 1(c)), almost completely disappear when the plasma response field is included (Fig. 1(d)), indicating strong resonant field screening inside the plasma and away from the plasma edge. Consequently, the magnetic field stochasticity is substantially reduced by the plasma response. This has a direct consequence on the RE loss properties reported below.

3.1. RMP configuration for best ELM control

Figure 2 compares the RE loss properties modeled by MARS-F, between the vacuum field approximation and that including the plasma response, assuming the best coil phasing for ELM control. We populate the initial (seeding) REs uniformly in the $\psi_p - \chi$ configuration space, with χ denoting the (equal-arc) poloidal angle. The particle phase space parameters are fixed to be mono-energy (25 MeV) and mono-pitch angle ($\lambda = 0.1$). Note that λ effectively denotes the particle magnetic moment. In a well-established runaway beam, REs are typically passing particles that are well-aligned with the magnetic field lines, i.e. with a small pitch angle λ. The parallel velocity of REs typically has a sign that is in counter-direction to the plasma current, i.e. $\sigma = \text{sign}(v_{||}) = -1$ in our convention. This is however not always the case for runaway seeds. In this study, we will always consider and compare REs with both signs of $\sigma = +1$ and $\sigma = -1$.

Figures 2 shows that the RE loss pattern is significantly different with or without taking into account the plasma response to the applied RMP field. The vacuum approximation leads to a rapid loss of REs, within 1 ms, that are launched outside the $\psi_p = 0.6$ surface (Fig. 2(a-b)). This is similar to what has been found in Ref. [11]. On the other hand, much less RE loss is found when the plasma response is included into the perturbed 3-D field (Fig. 2(c-d)). Note that this is despite the strong plasma induced amplification of $|\delta B|$ near the plasma edge. In fact, RE loss occurs only near the plasma edge region, with $\psi_p > 0.9$, when the total perturbation field is considered. Strong plasma screening of the resonant radial field components in the $\psi_p < 0.9$ region, as is evident from Fig. 1(d), is responsible for the much less RE loss in this region of plasma as compared to the vacuum field approximation.

The plasma response, on the other hand, does not significantly modify the wetted area hit by lost REs on the ITER limiting surface, as shown in Fig. 2(e-h). The lost REs in these cases aways hit the limiting surface at the poloidal angle of $\theta_{\text{eqac}} \sim 270^{\text{o}}$, corresponding to the lower divertor region (cf. Fig. 1(a-b)). Note that in this work, the poloidal angle of 0^{o} always denotes the outboard mid-plane. Too narrow wetted area is not a desirable feature for the RE loss. On the other hand, the simulated loss rate is generally low in particular when the plasma response is taken into account.

Figure 2 only shows the loss properties for 25 MeV REs. More examples, with

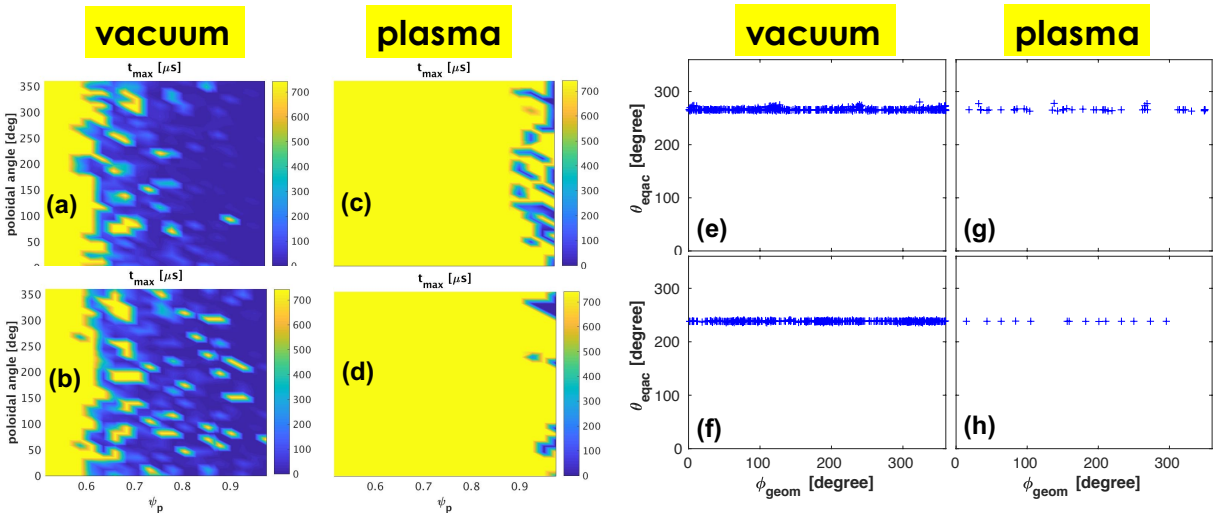

Figure 2. Comparison of the RE loss properties between (a,b,e,f) the case with the vacuum field approximation, and (c,d,g,h) the case with the total field perturbation including the plasma response. The contour plots in (a-d) show the simulation time (in μs) before the REs are lost to the ITER limiting surface or stay confined after reaching steady state. Plots (e-h) show the location of lost REs on the limiting surface, with $\theta_{\rm eqac} = 0^{\rm o}$ indicating the low-field side mid-plane. The REs are launched with a uniform initial distribution along the normalized poloidal magnetic flux ψ_p and the poloidal angle, with the same velocity pitch angle of $\lambda_0 = 0.1$ and the particle energy of 25 MeV. The initial parallel velocity of REs is assumed to be either co- (top panels) or counter- (bottom panels) to the equilibrium plasma current. The vacuum field is produced by three rows of the ELM control coils at 90 kAt coil current, with the $n = 3$ waveform and the coil phasing of ($200^{\rm o}$, $0^{\rm o}$, $140^{\rm o}$) for the upper, middle and lower rows, respectively, in an ITER 15 MA pre-disruption plasma.

varying RE energy, are reported in Fig. 3. Note that only results including the plasma response are shown here, since these represent more realistic predictions than that assuming the vacuum field approximation. Note also that low-energy REs, at 18.6 keV, are studied here as a special case. This corresponds to the maximum energy of electrons produced by beta-decay of the tritium nucleus. Tritium decay has been considered as one possible mechanism of runaway seeding in ITER D-T plasmas [8]. Figure 3 shows that the $n = 3$ RMP field induced RE loss occurs only near the plasma edge region, beyond $\psi_p = 0.9$ in the ITER 15 MA baseline plasma, independent of the particle energy. This also applies to REs produced by tritium decay. Interestingly, the loss fraction does not monotonically depend on the particle energy - slightly stronger loss occurs for the 10 MeV REs. This will be further quantified in a later figure.

The wetted area on the limiting surface, due to lost REs, is also not sensitive to the assumed particle energy. This is illustrated in Fig. 4. Most of the lost REs hit the lower divertor region of the limiting surface. Note that this holds for particles traveling in either direction along the magnetic field lines. This is somewhat different from the loss pattern due to the MHD instability in DIII-D or due to RMP in COMPASS [30],

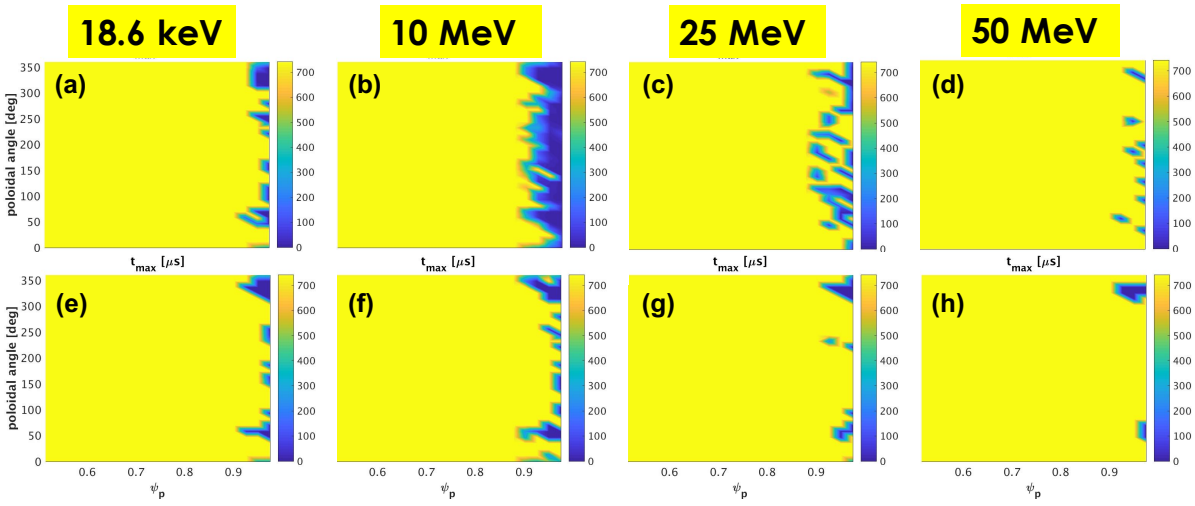

Figure 3. Contour plots showing the simulation time (in μs) before the REs are lost to the ITER limiting surface or stay confined after reaching steady state. The REs are launched, in the presence of RMP including the plasma response, with a uniform initial distribution along the normalized poloidal magnetic flux ψ_p and the poloidal angle, with the same velocity pitch angle of $\lambda_0 = 0.1$ and the particle energy of (a,e) 18.6 keV (seeding REs due to tritium decay), (b,f) 10 MeV, (c,g) 25 MeV, and (d,h) 50 MeV. The initial parallel velocity of REs is assumed to be either co- (top panels) or counter- (bottom panels) to the equilibrium plasma current. The RMP field is produced by three rows of the ELM control coils at 90 kAt coil current, with the $n = 3$ waveform and the coil phasing of (200°, 0°, 140°) for the upper, middle and lower rows, respectively, in an ITER 15 MA pre-disruption plasma.

where lost REs tend to hit either the LFS or HFS of the limiting surface.

The RE loss fraction, as a function of the simulation time, is quantified in Fig. 5. The loss fraction is defined as the ratio of the lost RE number (to the limiting surface) to the total number of REs that are initially launched from inside the plasma. The co-passing REs experience a slightly larger loss than the counter-passing particles. But the overall loss due to the RMP field is small after reaching the steady state - less than 8% in the best case for the 10 MeV co-passing REs. We emphasize that these results already assume the maximum coil current capacity in ITER - even lower RE loss rate is expected with smaller RMP fields. The steady state loss fraction is a non-monotonic function of the particle energy. In particular, 50 MeV high-energy REs experience less than 1% loss independent of the traveling direction. This trend (at higher particle energy) agrees with that from a previous modeling for DIII-D [20]. An heuristic understanding (supported by examining single particle trajectories) outlined in Ref. [20] is that higher-energy (MeV level) REs are less influenced by the 3-D perturbation field. Figure 5 also shows fast RE loss. In all cases, most of REs are lost to the limiting surface within $\sim 500\mu$s.

We make a comment here on the drift orbit approximation for high-energy REs. In order to properly describe dynamics of very high energy REs, say at 100 MeV level,

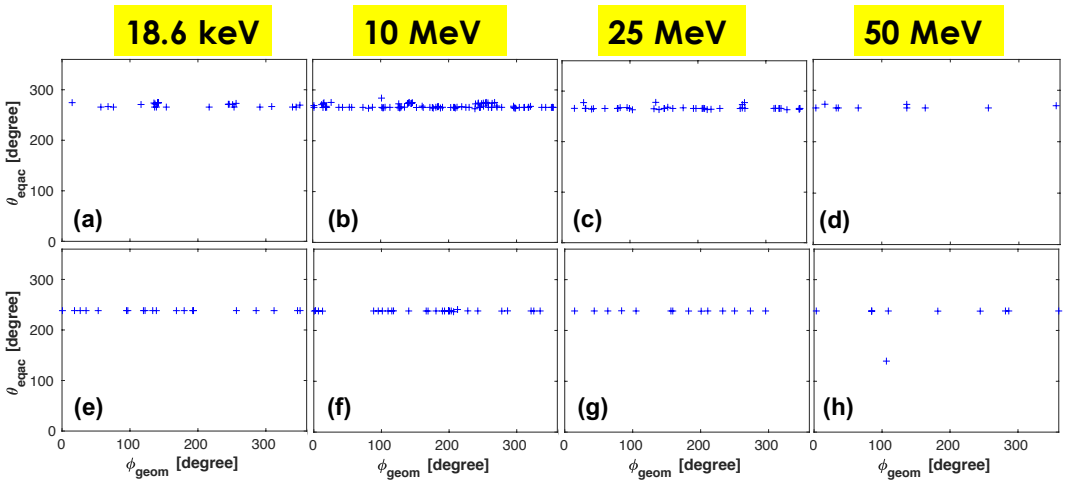

Figure 4. The location of lost REs on the ITER limiting surface, in the presence of RMP including the plasma response. The REs are launched with a uniform initial distribution along the normalized poloidal magnetic flux ψ_p and the poloidal angle, with the same velocity pitch angle of $\lambda_0 = 0.1$ and the particle energy of (a,e) 18.6 keV (seeding REs due to tritium decay), (b,f) 10 MeV, (c,g) 25 MeV, and (d,h) 50 MeV. The initial parallel velocity of REs is assumed to be either co- (top panels) or counter- (bottom panels) to the equilibrium plasma current. The RMP field is produced by three rows of the ELM control coils at 90 kAt coil current, with the $n = 3$ waveform and the coil phasing of (200°, 0°, 140°) for the upper, middle and lower rows, respectively, in an ITER 15 MA pre-disruption plasma.

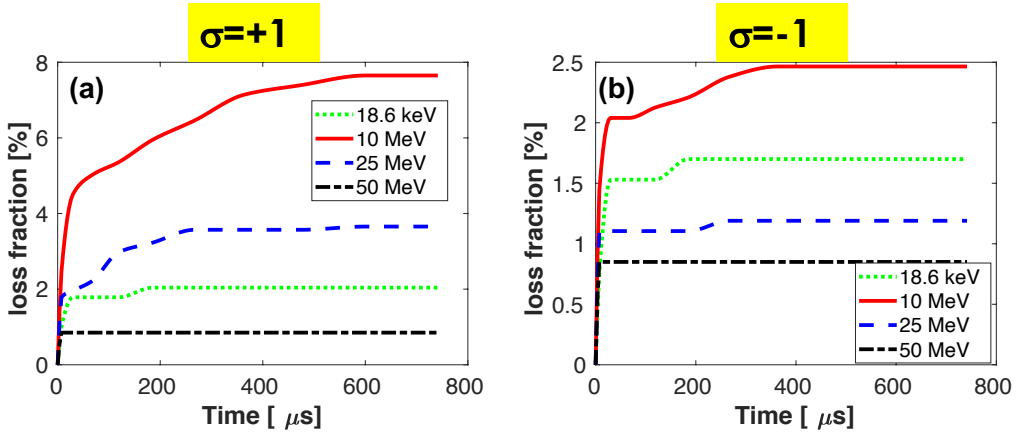

Figure 5. The RE loss fraction versus the simulation time, for particles launched with the initial parallel velocity being in either (a) co- or (b) counter-direction to the equilibrium plasma current. Considered are REs with the initial pitch angle of $\lambda_0 = 0.1$ and varying initial particle energy: 18.6 keV (seeding REs due to tritium decay), 10 MeV, 25 MeV, and 50 MeV. The RMP field is produced by three rows of the ELM control coils at 90 kAt coil current, with the $n = 3$ waveform and the coil phasing of (200°, 0°, 140°) for the upper, middle and lower rows, respectively, in an ITER 15 MA pre-disruption plasma.

full orbit model becomes essential [40, 41]. Drift orbit model, which is what we adopt in this study, may over-predict the particle loss at high-energies. A recent calculation that takes into account a gyro-orbit correction to the particle magnetic moment for high-energy REs [42] may help to improve the drift orbit model. This correction is not taken into account in the present REORBIT module. For the above reasons, we limit our scan of the RE energy up to 50 MeV, where the drift orbit approximation still holds reasonably well [41].

3.2. RMP configuration for worst ELM control

We have so far assumed the RMP spectrum that maximizes the plasma edge resonant response. For comparison, we now consider an opposite case that minimizes the quoted effect and thus leads to the worst ELM control according to Refs. [38, 39]. With the same ELM control coil current amplitude of 90 kAt, the corresponding coil phasing is (25°, 0°, 285°) for the upper, middle and lower rows, respectively. As illustrative examples, we again consider mono-energy REs at 25 MeV. Figure 6 shows a smaller RE loss region in the configuration space, assuming the vacuum field approximation (Fig. 6(a-b)). The loss region is now limited to $\psi_p > 0.7$, compared to the larger region covering $\psi_p > 0.6$ with the best coil phasing as shown in Fig. 2(a-b). With inclusion of the plasma response (Fig. 6(c-d)), no co-passing RE is lost and the loss region for counter-passing REs is very small. All the lost REs again hit the lower divertor region of the limiting surface (Fig. 6(e-h)), similar to that of the best coil phasing case shown in Fig. 2(e-h).

The results reported in Figs. 2 and 6 are summarized in Fig. 7, in the form of the RE loss fraction versus the simulation time. The saturated loss fraction is between 20-40% assuming the vacuum field model, in a similar range to that predicted in Ref. [11]. The loss fraction is however below 5% independent of the assumed RMP spectrum (at the same coil current of 90 kAt), when the plasma response is taken into account. This shows that the vacuum field approximation needs to be employed with caution when investigating the RE loss by RMP fields in ITER. On the other hand, at lower thermal electron temperature, the plasma response is expected to provide less shielding of the resonant field perturbation and consequently a larger RE loss. Although not reported here, we also considered a 15 MA equilibrium with vanishing plasma pressure. The modeled RE loss fraction, taking into account the plasma response to the RMP field, is about 25-30%, i.e. between the vacuum field and total response field results reported earlier (for the full pressure case). In general, taken into account the plasma response, MARS-F modeling shows that the RMP field is not effective in mitigating REs (or RE seeds) in ITER, even with the maximum ELM control coil current designed for ITER. This motivates another way of mitigating REs with 3-D fields, reported below.

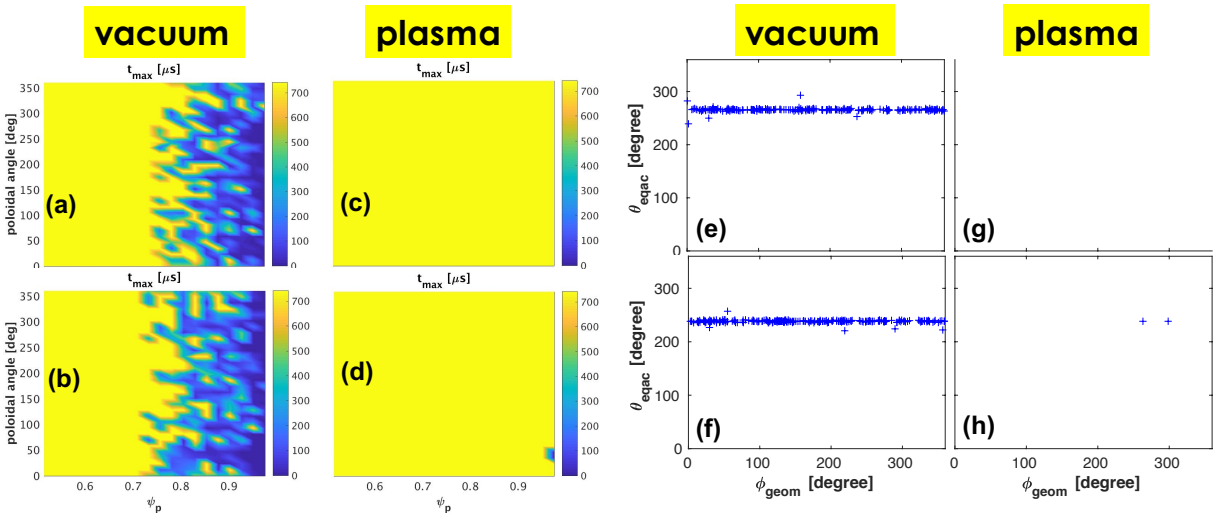

Figure 6. Comparison of the RE loss properties between (a,b,e,f) the case with the vacuum field approximation, and (c,d,g,h) the case with the total field perturbation including the plasma response. The contour plots in (a-d) show the simulation time (in μs) before the REs are lost to the ITER limiting surface or stay confined after reaching steady state. Plots (e-h) show the location of lost REs on the limiting surface. (Note that no RE is lost in (c,g) and plot (g) is kept only for completeness.) The REs are launched with a uniform initial distribution along the normalized poloidal magnetic flux ψ_p and the poloidal angle, with the same velocity pitch angle of $\lambda_0 = 0.1$ and the particle energy of 25 MeV. The initial parallel velocity of REs is assumed to be either co- (top panels) or counter- (bottom panels) to the equilibrium plasma current. The vacuum field is produced by three rows of the ELM control coils at 90 kAt coil current, with the $n = 3$ waveform and the coil phasing of (25°, 0°, 285°) for the upper, middle and lower rows, respectively, in an ITER 15 MA pre-disruption plasma.

4. RE loss due to MHD instabilities

As mentioned earlier, DIII-D and JET experiments have demonstrated effective purging of REs relying on the naturally occurring $n = 1$ MHD instabilities, when the plasma edge safety factor is sufficiently low [15, 20, 35–37]. In what follows, we investigate whether this mechanism also works for ITER. For this purpose, we consider a series of ITER post-thermal quench equilibria simulated by the DINA code [26, 27]. The plasma disruption in this DINA simulation is triggered by injecting neon impurity into the plasma. The disruption simulation was performed again for an ITER plasma from the 15 MA baseline scenario.

4.1. MHD instabilities during disruption

Current-driven, low-n MHD instabilities often occur in a post-disruption plasma when nq_a (q_a is the edge safety factor) evolves below an integer number. Note that a post-thermal quench plasma typically has very low thermal pressure. The pressure-driven MHD instabilities are therefore not expected. In what follows, we consider the $n = 1$

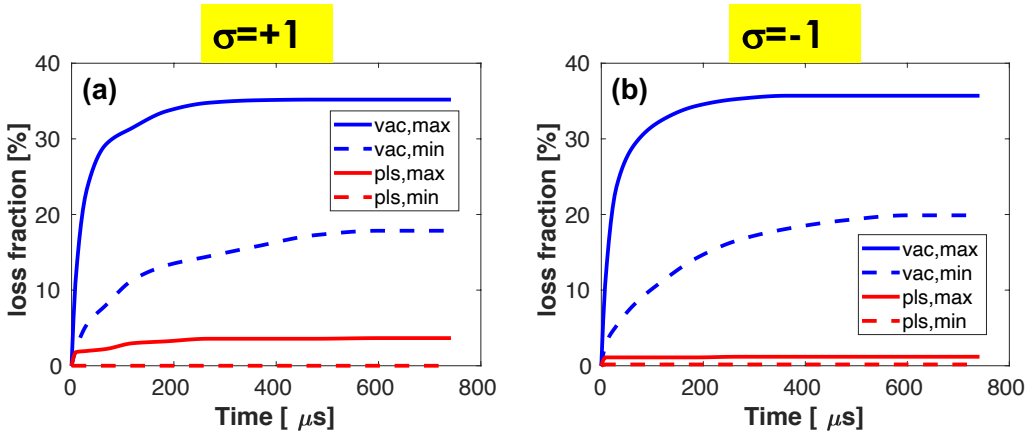

Figure 7. Comparison of the RE loss fraction versus the simulation time, for particles launched with the initial parallel velocity being in either (a) co- or (b) counter-direction to the equilibrium plasma current, and in the presence of different perturbation fields produced by three rows of the ELM control coils at 90 kAt coil current and with the $n = 3$ waveform: the vacuum field alone (curves in blue) or the total field including the plasma response (curves in red). Solid curves assume the coil phasing of (200°, 0°, 140°) and dashed curves assume the coil phasing of (25°, 0°, 285°), for the upper, middle and lower rows, respectively, in an ITER 15 MA pre-disruption plasma. Considered are REs with the initial pitch angle of $\lambda_0 = 0.1$ and the particle energy of 25 MeV.

instabilities for three equilibria from the time-dependent DINA simulation. These were chosen at the time steps with q_a (defined at the last closed flux surface) successively drops below 4,3 and 2, as the plasma volume shrinks during the current quench (Fig. 8(a)). The relevant equilibrium parameters are listed in Table 1. This VDE resembles Case 1 from Ref. [24] and has the same width and amplitude of the initial RE seed: w=0.5 and $I_{\rm seed}$=1.5 MA. Note that the chosen equilibria correspond to later stages of the disruption, when a significant fraction of the plasma current is already carried by REs. Note also that these plasmas, effectively representing runaway beams, are in the limiter configuration (with surrounding halo currents which we neglected). Therefore, the edge safety factor q_a (instead of the q_{95} value which is typically more relevant for divertor plasmas) is listed in Table 1. The radial profiles of the safety factor are plotted in Fig. 8(b).

MARS-F finds linearly unstable $n = 1$ resistive kink modes for these equilibria, with the growth rates also documented in Table 1. The Lundquist number is assumed to be 10^5 in these MARS-F computations, which corresponds to the typical value for these post-thermal quench, low thermal electron temperature plasmas in ITER. We point out that, as in Ref. [20], these resistive kink instabilities are associated with the bulk (thermal) plasma. The runaway electrons, representing a minority particle population, on the other hand contribute a large fraction of the equilibrium current. Therefore, generally speaking, a MHD-RE hybrid model is needed, in order to properly describe the stability of such a runaway beam plasma. Such models have recently

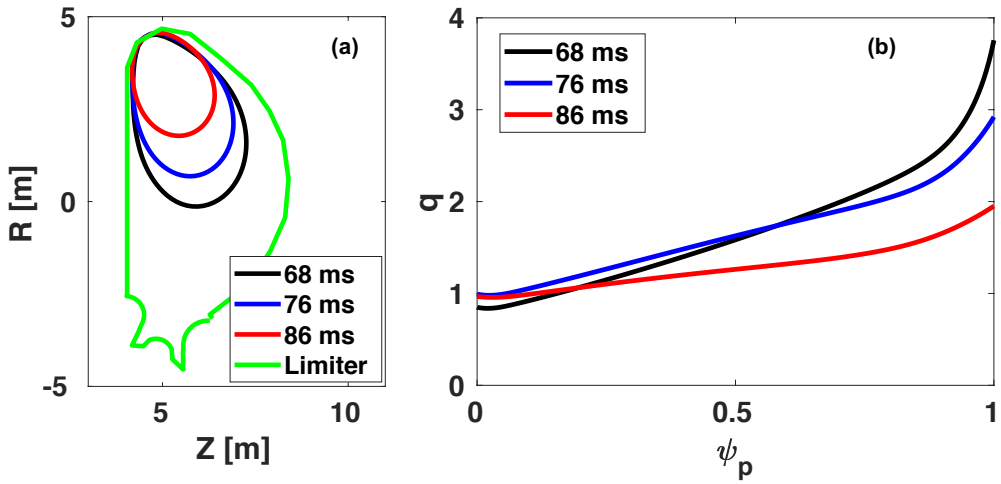

Figure 8. Equilibria from three time slices (68 ms, 76 ms and 86 ms) during the DINA-simulated disruption mitigation by injecting impurity (neon) into an ITER plasma from the 15 MA baseline scenario. Shown in (a) are the plasma boundary shapes together with the ITER limiting surface, and (b) the corresponding safety factor profiles for these three equilibria.

Table 1. Chosen equilibria at three time slices from the DINA disruption simulation for an ITER 15 MA plasma, with the associated $n = 1$ resistive kink instability computed by MARS-F. I_p is the equilibrium plasma current with $I_{\rm RE}$ denoting the portion carried by runaway electrons. q_0 and q_a are the on-axis and edge safety factors, respectively. γ is the resistive kink growth rate normalized by the toroidal Alfvén time τ_A.

time (ms)	I_p (MA)	$I_{\rm RE}$ (MA)	q_0	q_a	$\gamma\tau_A$
68	8.39	7.97	0.85	3.76	2.29×10^{-2}
76	7.93	7.30	0.99	2.92	1.00×10^{-2}
86	6.97	6.08	0.97	1.95	3.12×10^{-2}

been developed [30, 43–46]. In this study, we nevertheless adopt the fluid model, which shows a reasonably good agreement with experiments in DIII-D, in terms of both the instability time scale and the resulting RE loss properties [15, 20, 30]. Furthermore, a recent modeling work employing the hybrid model shows that, at least for the internal kink instability, the effect due to the RE induced modification to the mode eigenfunction on the RE loss is not substantial [46].

The MARS-F computed fluid mode eigenfunctions are shown in Figs. 9 and 10, for the plasma displacement and the perturbed field amplitude, respectively. It is evident that the mode structures are significantly different at different time slices. This is mainly dictated by the safety factor profiles for these current-driven instabilities. At 68 ms, when the edge safety factor is below 4, the on-axis value is well below 1 ($q_0 = 0.85$), resulting in a resistive internal kink instability with the $m = 1$ dominant poloidal

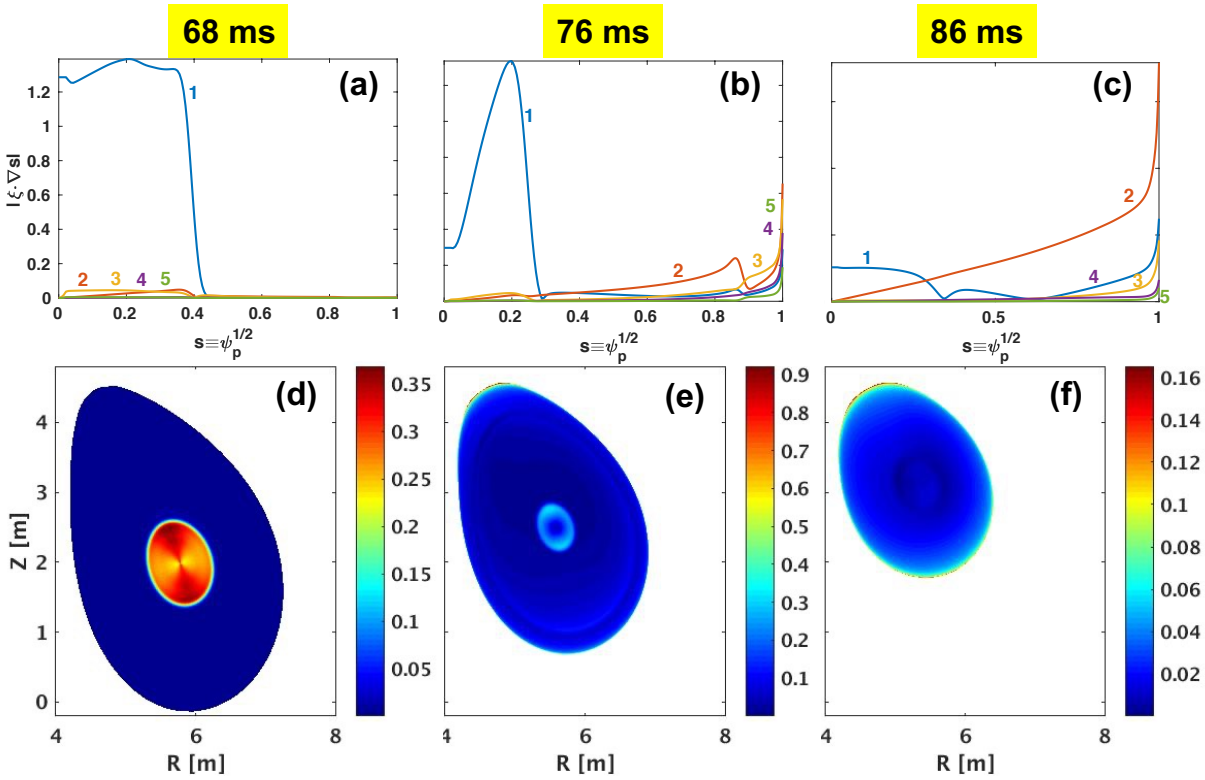

Figure 9. Eigenfunctions of the $n = 1$ unstable resistive kink modes, computed by MARS-F for the ITER post-disruption equilibria at 68 ms (left panels), 76 ms (middle panels) and 86 ms (right panels). Plotted are (a-c) the poloidal Fourier harmonics ($m = 1 - 5$ as the dominant portion of the poloidal spectrum) of the plasma radial displacement, and (d-f) amplitude of the radial displacement on the poloidal cross-section.

harmonic (Fig. 9(a)). Both the plasma displacement (Fig. 9(d)) and the magnetic field perturbation (Fig. 10(a)) are mainly located within the $q = 1$ surface. Note that the ideal internal kink is stable in this case, due to the Bussac stabilization and the lack of pressure drive [47]. We point out that the resistive kink eigenfunction at 76 ms is qualitatively similar to that identified for the DIII-D experiments [15, 20]. This is different from the double tearing mode identified for JET [36].

At 76 ms when q_a is just below 3, the eigenmode contains both the internal kink component ($m = 1$) in the plasma core and external kink components ($m = 5, 4, ...$) near the plasma edge (Fig. 9(b)). The plasma radial displacement and the perturbed field, as shown on the poloidal plane in Figs. 9(e) and 10(b), respectively, are large both within the $q = 1$ surface and near the plasma edge. As will be shown later on, this rich spectrum in the 3-D perturbation is favorable for RE mitigation. We mention that the idea kink mode is also unstable in this case, with slightly lower growth rate than that of the resistive counterpart. For the post-thermal quench plasma with low thermal electron temperature, the resistive kink instability represents a physically more relevant solution here.

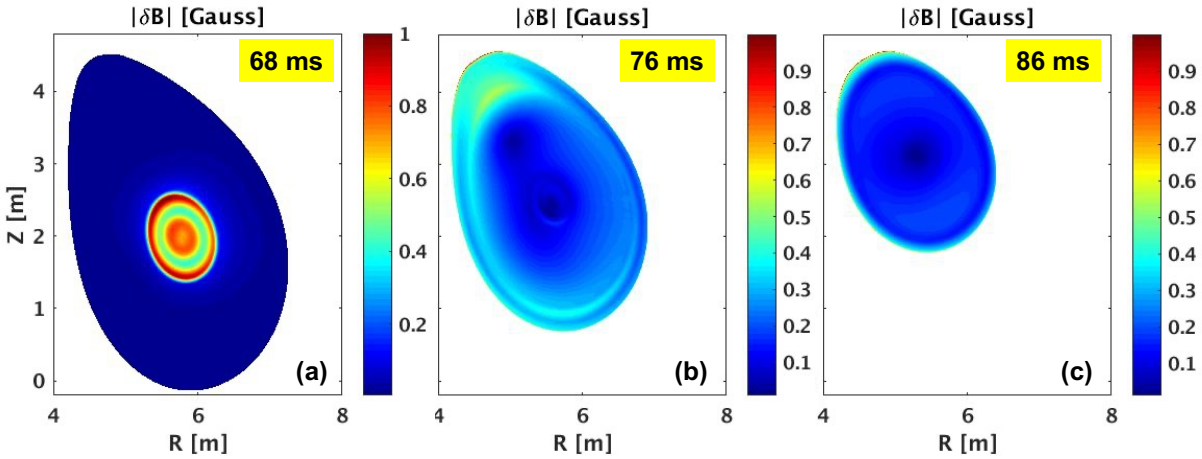

Figure 10. Amplitude of the perturbed magnetic field perturbation inside the plasma, associated with the $n = 1$ resistive kink instabilities for the ITER post-disruption equilibria at (a) 68 ms, (b) 76 ms and (c) 86 ms, respectively, and plotted on the poloidal cross-section. The peak value of the perturbation amplitude over the plasma volume is normalized to unity (1 Gauss) here.

At 86 ms when q_a is just below 2, the instability has the largest growth rate (Table 1), but most of the perturbation is located in the plasma edge region (Figs. 9(f) and 10(c)). The instability mainly resembles an external kink mode, with the $m = 2$ dominant poloidal harmonic in this case (Fig. 9(c)). Note that the $n = 1$ ideal external kink is again unstable for this equilibrium, with nearly identical eigenmode structure as that of the resistive counterpart. Note that a similar case, with the same RE seed, was also found to be accompanied with an unstable (2,1) mode during the whole course of the VDE [24].

We emphasize that Figs. 9 and 10 only show and compare the eigenmode structure. The overall amplitude of the eigenfunction has no physical significance in a linear eigenvalue problem. The eigenfunction amplitude is thus scaled in such a way, that the peak amplitude of the perturbed magnetic field is unity (1 Gauss) as shown in Fig. 10 for all three cases. For the RE loss study, to be reported below, the overall amplitude of the perturbation of course matters. The perturbation amplitude cannot be predicted by a linear stability code such as MARS-F (and no experimental data is yet available for ITER). We will therefore scale the overall perturbation amplitude in Figs. 9 and 10 by a numerical factor. We start by assuming a numerical factor of 9.4×10^3, resulting in peak field perturbation amplitude of 9.4 kG. This will be referred to as the 9.4 kG perturbation field. This perturbation level corresponds to the same value of $|\delta B/B_0| = 0.18$ as assumed for modeling the MHD-induced RE loss in DIII-D [20]. The experimentally measured $n = 1$ perturbation level is at a similar range, when mapped to the sensor location at the high-field side wall [20]. We mention that this level of perturbation was found experimentally to be capable of completely de-confining the runaway current beam in DIII-D [15].

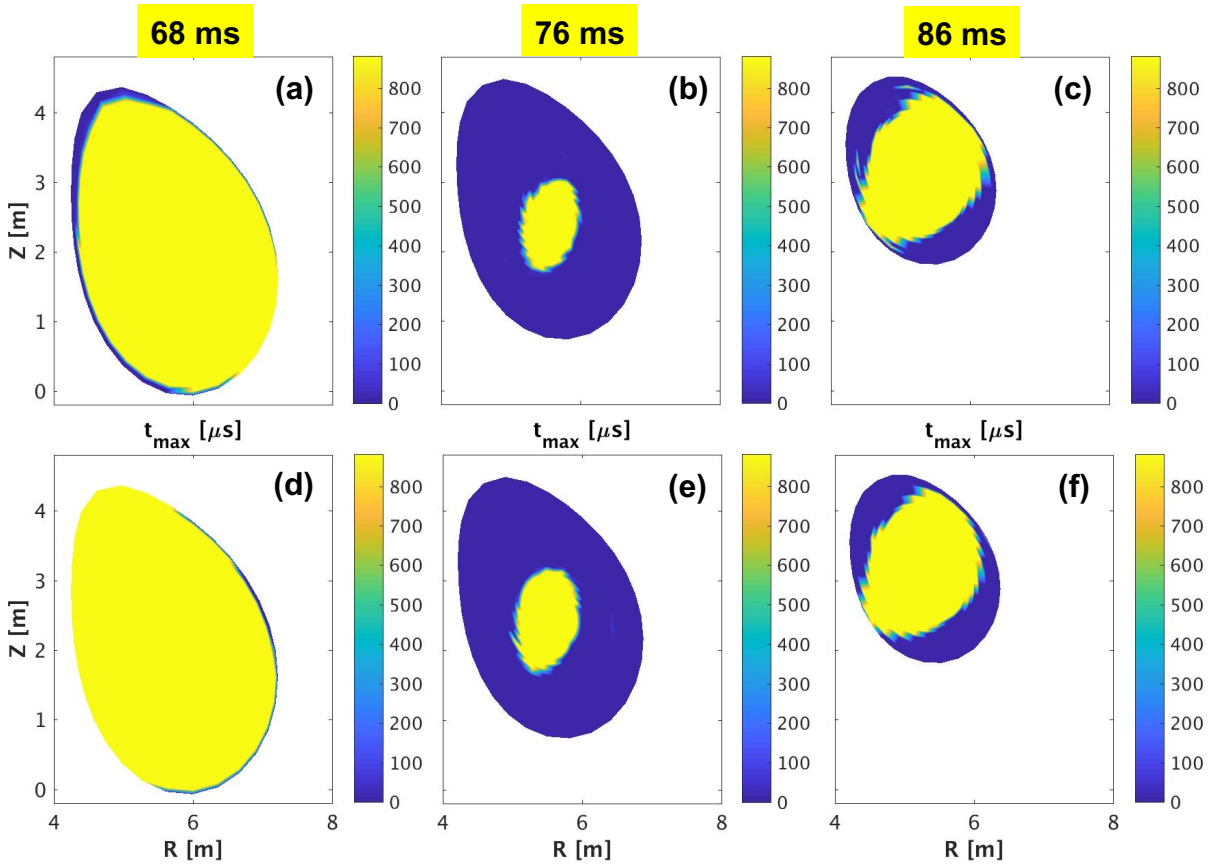

Figure 11. Contour plots showing the simulation time (in μs) before the REs are lost to the ITER limiting surface or stay confined after reaching steady state, in the presence of 3-D perturbations due to the $n = 1$ resistive kink instabilities in the post-disruption ITER plasmas at 68 ms (left panels), 76 ms (middle panels), and 86 ms (right panels), respectively. The REs are launched on the poloidal cross-section with a uniform initial distribution along the normalized poloidal magnetic flux ψ_p and the poloidal angle, with the same velocity pitch angle of $\lambda_0 = 0.1$ and the particle energy of 50 MeV. The initial parallel velocity of REs is assumed to be either (a-c) co- or (d-f) counter-direction to the equilibrium plasma current. The peak value of the perturbed magnetic field amplitude over the plasma volume is assumed to be 9.4 kG in all three cases.

4.2. RE loss with 9.4 kG perturbation field

In this subsection, the peak perturbation amplitude $|\delta B|$ inside the plasma is assumed to be 9.4 kG in all three cases at 68 ms, 76 ms and 86 ms. Mono-pitch angle ($\lambda = 0.1$) and mono-energy (but with different choices of values) REs are launched from inside the plasma, with a uniform initial distribution along the radial coordinate ψ_p and the (equal-arc) poloidal angle. Figures 11 and 12 reports the simulation results for 50 MeV REs, where the RE loss pattern is presented either on the poloidal cross-section or along the radial and poloidal coordinates.

Two key observations can be made. First, at the same overall perturbation

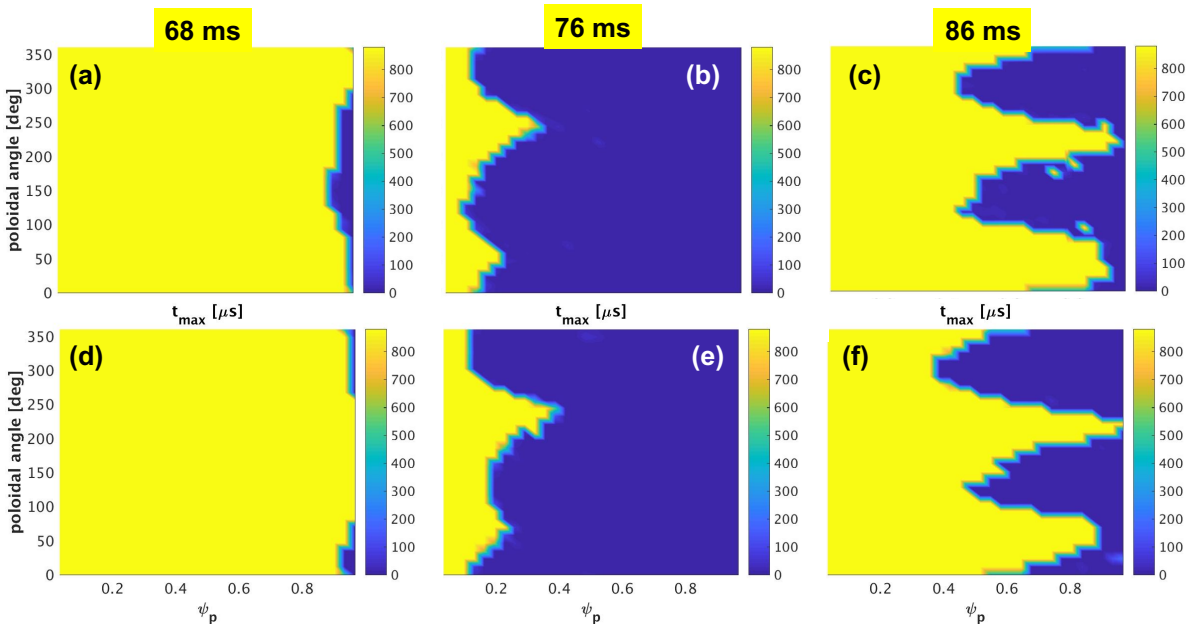

Figure 12. Contour plots showing the simulation time (in μs) before the REs are lost to the ITER limiting surface or stay confined after reaching steady state, in the presence of 3-D perturbations due to the $n = 1$ resistive kink instabilities in the post-disruption ITER plasmas at 68 ms (left panels), 76 ms (middle panels), and 86 ms (right panels), respectively. The REs are launched with a uniform initial distribution along the normalized poloidal magnetic flux ψ_p and the poloidal angle, with the same velocity pitch angle of $\lambda_0 = 0.1$ and the particle energy of 50 MeV. The initial parallel velocity of REs is assumed to be either (a-c) co- or (d-f) counter-direction to the equilibrium plasma current. The peak value of the perturbed magnetic field amplitude over the plasma volume is assumed to be 9.4 kG in all three cases.

amplitude, the RE loss is rather sensitive to the details in the unstable MHD eigenmode structure. The core-localized instability shown in Fig. 9(a,d), i.e. the resistive internal kink at 68 ms, is not effective in purging REs even at a large perturbation amplitude (Figs. 11(a,d) and 12(a,d)). In fact, only REs launched from the very edge of plasma (beyond the $\psi_p = 0.9$ surface) are lost to the limiting surface. This agrees with the conclusion reached in a recent study (for a generic toroidal equilibrium) where a MHD-RE hybrid model is employed to describe the internal kink instability [46]. We mention that experimental results of RE loss from internal kink in DIII-D also support this conclusion [21]. The external kink instability, not surprisingly, is more efficient to purge REs. The loss is not uniform for particles launched along the poloidal angle, as is evident from Figs. 11(c,f) and 12(c,f). At poloidal angles of $\sim 120^o$ and $\sim 300^o$, particles located as deep as $\psi_p = 0.5$ are eventually lost to the limiting surface due to the $n = 1$ resistive external kink instability.

The most efficient loss, however, occurs when the mode eigenfunction is global and contains both internal and external kink components (Figs. 11(b,e) and 12(b,e)). REs located in the plasma core region ($\psi_p \sim 0.2$) are also lost due to the $n = 1$ MHD

instability in this case. Furthermore, the loss pattern experiences less variation along the poloidal angle. These results show that, for successful purge of REs in a post-disruption runaway beam, it is important that the MHD perturbation is global, covering both the core and edge regions of the plasma. In the simulated ITER scenario, this occurs when q_a drops just below 3. We point out that in DIII-D experiments, this kind of MHD perturbation with mixed kink components occurs when q_a is slightly above 2. In general, the poloidal spectrum of the current-driven resistive kink strongly depends on the radial profile of the safety factor, in particular on the q_0 and q_a values. For instance, for the chosen ITER equilibrium at 86 ms with q_a just below 2 (Table 1), the 2/1 external kink component becomes predominant, effectively "over-shadows" the 1/1 internal kink component despite the fact that q_0 is slightly below 1 in this case. This is because, for a limiter plasma, a strong drive of external kink occurs when the edge safety factor is just below an integer number (for the $n = 1$ perturbation). On the contrary, the DIII-D equilibrium reported in Ref. [20] has q_a just above 2. This results in a weaker 2/1 external kink component. As a consequence, the 1/1 internal component also becomes prominent, despite that q_0 is slightly above 1 in this case.

Secondly, even with the most favorable mode eigenfunction (Figs. 9(b,e)), no complete RE purge occurs in ITER at 9.4 kG perturbation level. This is different from DIII-D with the similar mode structure and with the same level of $|\delta B|/B_0$, where all REs are lost to the limiting surface [30]. One possible reason is that the position of the RE beam was intentionally controlled in DIII-D, to be located at the mid-plane near the center-post, whilst the beam is located near the upper corner in ITER. The relative location of the RE beam with respect to the limiting surface also affects the efficiency of RE purge by 3-D fields. Nevertheless, Figs. 11(b,e) and 12(b,e) show a substantial fraction ($\sim 80\%$) of RE loss, which is a promising result for ITER.

The wetted area due to lost REs hitting the ITER limiting surface also depends on the eigenmode structure, as demonstrated in Fig. 13. With the resistive internal kink instability, the lost co-passing REs tend to hit the divetor region of the limiting surface ($\theta_{\rm eqac} \sim 300^{\rm o}$, Fig. 13(a)). The counter-passing REs on the other hand mainly hit the top of the limiting surface ($\theta_{\rm eqac} \sim 100^{\rm o}$, Fig. 13(d)). On the other hand, a much wider wetted area is achieved at 76 ms (Fig. 13(b,e)), when a more global resistive kink instability develops in the runaway beam plasma with the edge safety factor drops just below 3. This will be further quantified in the next figure. We note also that the wetted area becomes narrower at 86 ms, as q_a drops below 2 and the resistive external kink instability develops with small internal component (Fig. 13(c,f)). Figure 13 thus shows that a more global perturbation structure helps not only to purge REs but also to expand the wetted area on the limiting surface for this ITER scenario.

The RE loss due to MHD instabilities occurs very quickly in these ITER plasmas, as shown in Fig. 14(a-b), where we plot the loss fraction as a function of the simulation time. The steady state is reached after about 20 μs. This is the similar time scale for the runaway current dissipation by the MHD instability in DIII-D, according to both modeling [30] and experiments [15]. Within this fast time scale, the particle energy and

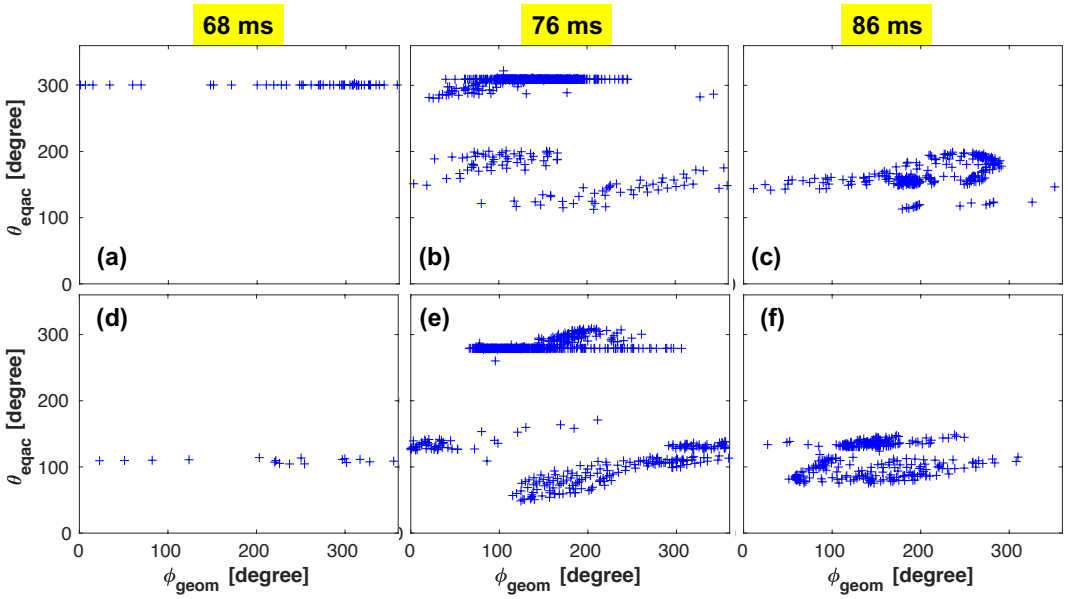

Figure 13. The location of lost REs on the ITER limiting surface, in the presence of 3-D perturbations due to the $n = 1$ resistive kink instabilities in the post-disruption ITER plasmas at 68 ms (left panels), 76 ms (middle panels), and 86 ms (right panels), respectively. The REs are launched with a uniform initial distribution along the normalized poloidal magnetic flux ψ_p and the poloidal angle, with the same velocity pitch angle of $\lambda_0 = 0.1$ and the particle energy of 50 MeV. The initial parallel velocity of REs is assumed to be either (a-c) co- or (d-f) counter-direction to the equilibrium plasma current. The peak value of the perturbed magnetic field amplitude over the plasma volume is assumed to be 9.4 kG in all three cases.

pitch angle do not experience a significant change due to the electric field and various scattering or dragging mechanisms. The latter thus play a limited role in the RE loss reported here.

As mentioned earlier, about 80% REs are lost to the limiting surface at steady state as q_a drops below 3 (at 76 ms), when a resistive instability develops that has a mixed structure of both internal and external kink components. The RE mitigation is less efficient, at $\sim 35\%$ level, with a resistive external kink instability as q_a approaches 2. At the same overall perturbation amplitude of 9.4 kG, the resistive internal kink is not at all effective in mitigating REs in ITER post-disruption plasmas.

The distributions of the lost REs along the poloidal circumference of the limiting surface are compared in Fig. 14(c-d). The loss distribution function here is constructed by counting the number all lost particles shown in Fig. 13 along the toroidal angle, at a given poloidal location on the limiting surface. This is then divided by the total number of lost REs and scaled to unity for the peak value of the distribution function (to facilitate comparison among different cases). Figure 14(c-d) shows that the lost REs mainly hit either the inboard side of the limiting surface, or a narrow region near the outer divertor. The wetted area in the poloidal angle, where the distribution function has finite value, covers about 50% at 76 ms, 30% at 86 ms, and less than 10% at 68 ms.

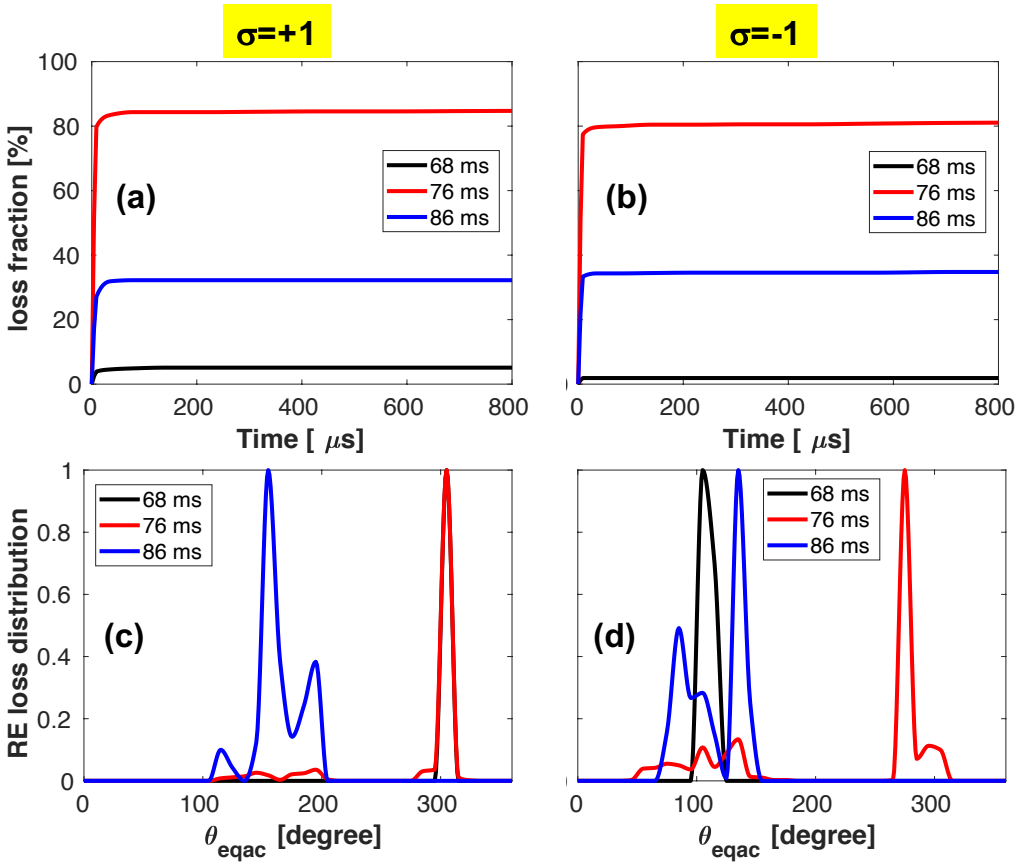

Figure 14. Comparison of (a-b) the RE loss fraction versus the simulation time, and (c-d) the final distribution of lost REs along the poloidal angle of the ITER limiting surface, for particles launched with the initial parallel velocity being in either (a,c) co- or (b,d) counter-direction to the equilibrium plasma current. In the presence are 3-D perturbations due to the $n = 1$ resistive kink instabilities in the post-disruption ITER plasmas at 68 ms (left panels), 76 ms (middle panels), and 86 ms (right panels), respectively, with the same peak value of $|\delta B| = 9.4$ kG over the plasma volume in all cases. $\theta_{\rm eqac} = 180^{\rm o}$ and $270^{\rm o}$ correspond to the high-field side and bottom of the limiting surface, respectively. Considered are REs with the initial pitch angle of $\lambda_0 = 0.1$ and the particle energy of 50 MeV.

The above results are obtained assuming 50 MeV REs. Similar studies have also been carried out for different choices of the particle energy level. The results show that the RE loss due to MHD instabilties, as well as the resulting wetted area on the limiting surface, is generally not sensitive to the particle energy. This is demonstrated by Fig. 15, where we compare the loss patterns for 10 MeV, 25 MeV, and 50 MeV REs at 76 ms, when the MHD perturbation is most effective in mitigating REs as compared to other two time slices. The overall loss fraction is nearly the same for all three particle energy levels. As will be reported later on, the loss pattern experiences slightly more variation with particle energy with the other two types of MHD instabilities (at 68 ms and 86 ms), but the general trend remains similar.

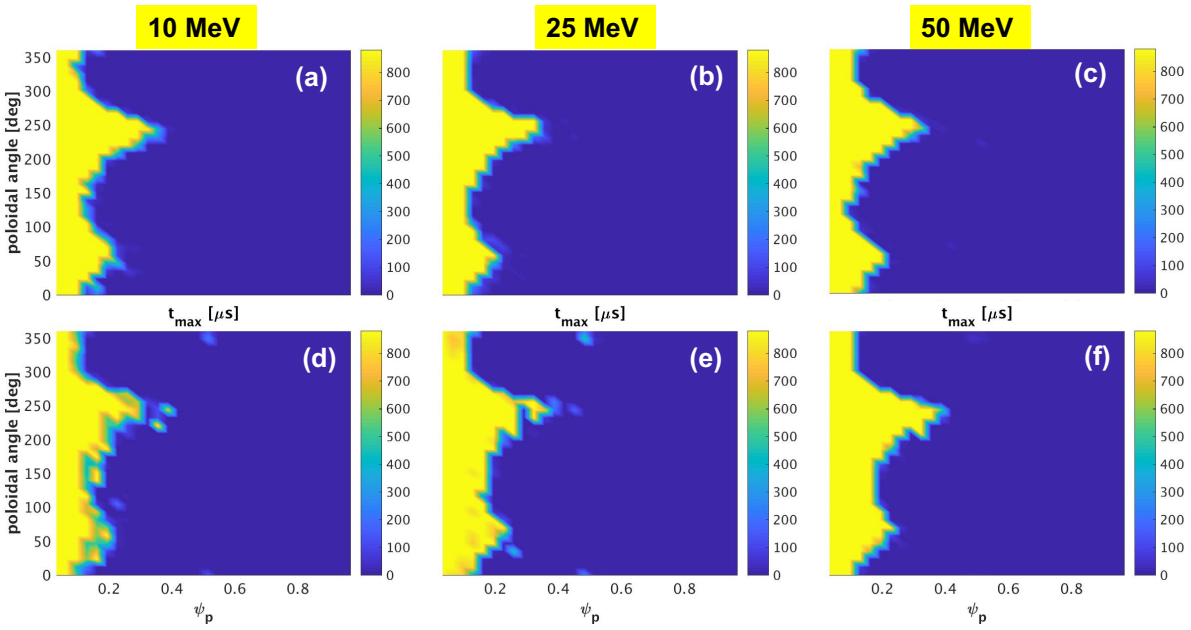

Figure 15. Contour plots showing the simulation time (in μs) before the REs are lost to the ITER limiting surface or stay confined after reaching steady state, in the presence of 3-D perturbations due to the $n = 1$ resistive kink instabilities in the post-disruption ITER plasma at 76 ms, when q_a drops below 3. The REs are launched with a uniform initial distribution along the normalized poloidal magnetic flux ψ_p and the poloidal angle, with the same velocity pitch angle of $\lambda_0 = 0.1$ and the particle energy of (a,d) 10 MeV, (b,e) 25 MeV, and (c,f) 50 MeV. The initial parallel velocity of REs is assumed to be either (a-c) co- or (d-f) counter-direction to the equilibrium plasma current. The peak value of the perturbed magnetic field amplitude over the plasma volume is assumed to be 9.4 kG in all cases.

4.3. RE loss with 18.8 kG perturbation field

Results reported in the previous subsection do not show full suppression of the runaway beam due to MHD instabilities, at the perturbation level of 9.4 kG. In this subsection, we consider the possibility of full RE purge by further increasing the perturbation level. More specifically, we consider doubling of the overall perturbation amplitude, to 18.8 kG. The modeling results are reported in Figs. 16-18, again for 50 MeV REs.

Not surprisingly, higher perturbation leads to higher RE loss for all three time slices considered in this work. The key finding is that now almost all REs are lost to the limiting surface at 76 ms (Fig. 16(b,e)), due to the $n = 1$ global resistive kink instability that occurs as q_a drops just below 3. We emphasize that our modeling does not inform whether a perturbation level of 18.8 kG is achievable in ITER. Non-linear MHD (or MHD-RE hybrid) simulations are needed to answer this question. In terms of $|\delta B|/B_0 (= 0.36)$, this level appears to be achievable according to the experimental observations in DIII-D [15]. Our modeling results shown here reveal the lower bound for the perturbation amplitude, that is needed to completely purge the RE beam in the ITER 15 MA baseline scenario. Note that our estimate for the lower bound may be

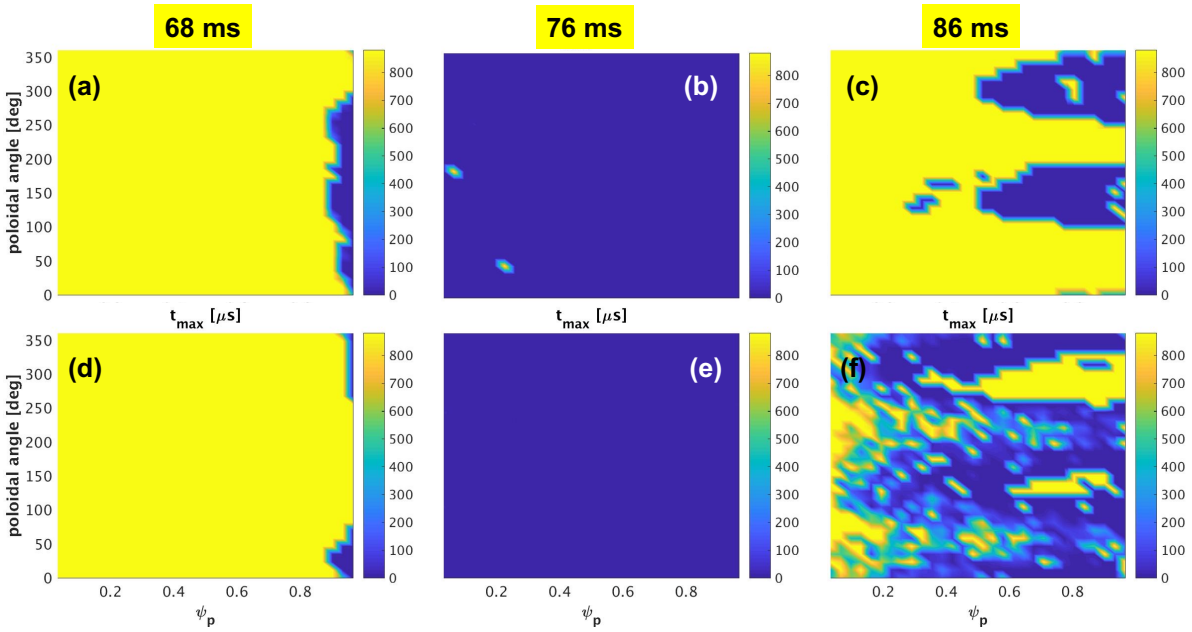

Figure 16. Contour plots showing the simulation time (in μs) before the REs are lost to the ITER limiting surface or stay confined after reaching steady state, in the presence of 3-D perturbations due to the $n = 1$ resistive kink instabilities in the post-disruption ITER plasmas at 68 ms (q_a below 4, left panels), 76 ms (q_a below 3, middle panels), and 86 ms (q_a below 2, right panels), respectively. The REs are launched with a uniform initial distribution along the normalized poloidal magnetic flux ψ_p and the poloidal angle, with the same velocity pitch angle of $\lambda_0 = 0.1$ and the particle energy of 50 MeV. The initial parallel velocity of REs is assumed to be either (a-c) co- or (d-f) counter-direction to the equilibrium plasma current. The peak value of the perturbed magnetic field amplitude over the plasma volume is assumed to be 18.8 kG in all three cases.

somewhat conservative. In reality, what can happen is that a significant portion of RE are purged as q_a drops below 3, and the residual REs may be mitigated by the external kink instability as q_a further evolves and drops below 2.

The loss patterns on the limiting surface, shown in Fig. 17, are similar to that at the 9.4 kG perturbation level (Fig. 13). The wetted area is slightly increased with doubling of the perturbation amplitude. The loss fraction and the loss distribution on the limiting surface are reported in Fig. 18 for the 18.8 kG perturbation case. Note that at 76 ms, 100% steady state loss fraction is achieved for REs traveling in both directions. The loss is still negligible at 68 ms. Up to 75% loss occurs for the counter-passing REs at 86 ms with the 18.8 kG perturbation - a significant increase compared to the $\sim 35\%$ loss fraction due to the 9.4 kG perturbation. This loss enhancement, however, does not happen for the co-passing particles, as is also evident by comparing Figs. 12(c) and 16(c).

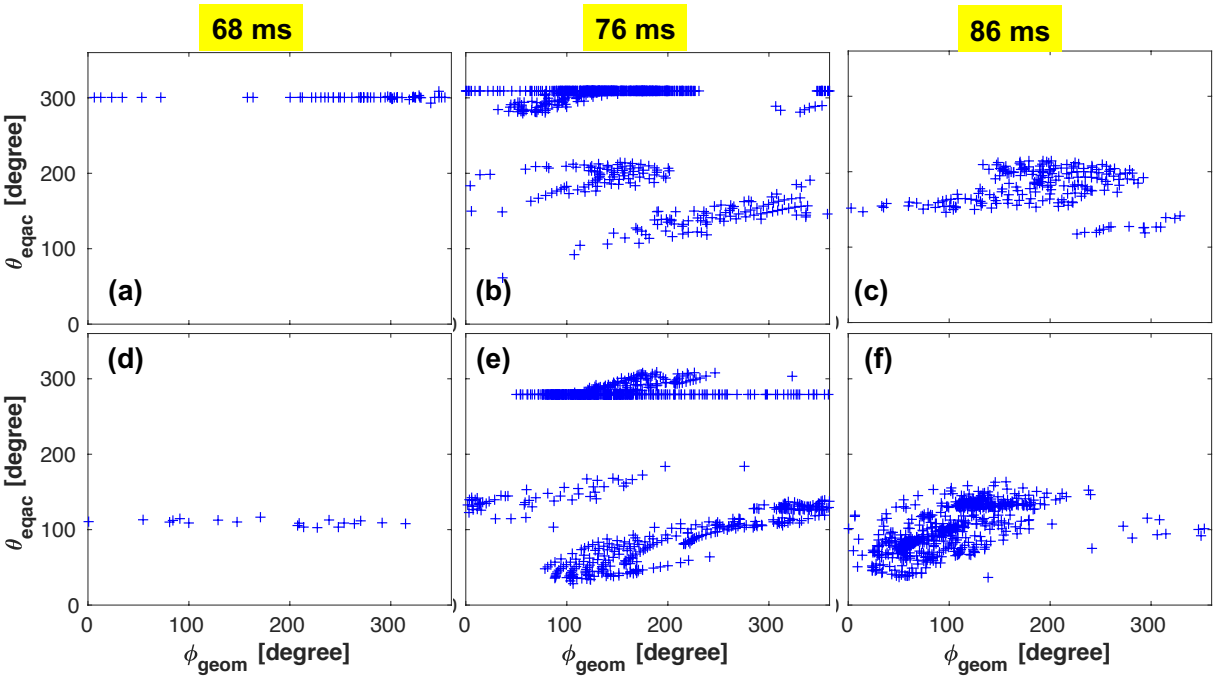

Figure 17. The location of lost REs on the ITER limiting surface, in the presence of 3-D perturbations due to the $n = 1$ resistive kink instabilities in the post-disruption ITER plasmas at 68 ms (q_a below 4, left panels), 76 ms (q_a below 3, middle panels), and 86 ms (q_a below 2, right panels), respectively. The REs are launched with a uniform initial distribution along the normalized poloidal magnetic flux ψ_p and the poloidal angle, with the same velocity pitch angle of $\lambda_0 = 0.1$ and the particle energy of 50 MeV. The initial parallel velocity of REs is assumed to be either (a-c) co- or (d-f) counter-direction to the equilibrium plasma current. The peak value of the perturbed magnetic field amplitude over the plasma volume is assumed to be 18.8 kG in all three cases.

4.4. RE loss with varying field perturbation

We have also modeled the RE loss at lower perturbation levels (1 kG and 5 kG) for this ITER scenario. The overall comparison, assuming various field amplitude, is shown in Fig. 19 for 50 MeV REs at 76 ms as one example. Only about 10% RE loss fraction is achieved with an 1 kG perturbation inside the plasma. Over 60% loss fraction is achieved with a 5 kG resistive kink perturbation. 100% suppression of REs, however, does require a tesla-level perturbation field in ITER. On the other hand, such a perturbation level, in terms of $|\delta B|/B_0$, has been shown to be achievable in DIII-D. An important reason, that this kind of perturbation can achieve large amplitude, is the kink nature of the underlying MHD instability which (i) is global and (ii) has large growth rate being comparable to that of an ideal kink. Both features ensure that the mode can hardly non-linearly saturate at its early stage of evolution.

Independent of the magnetic field perturbation level, the lost REs tend to hit similar areas of the limiting surface - either on the inboard side or near the outer divertor region (Fig. 19(c-d)). In particular, the strike points are mainly located near the outer

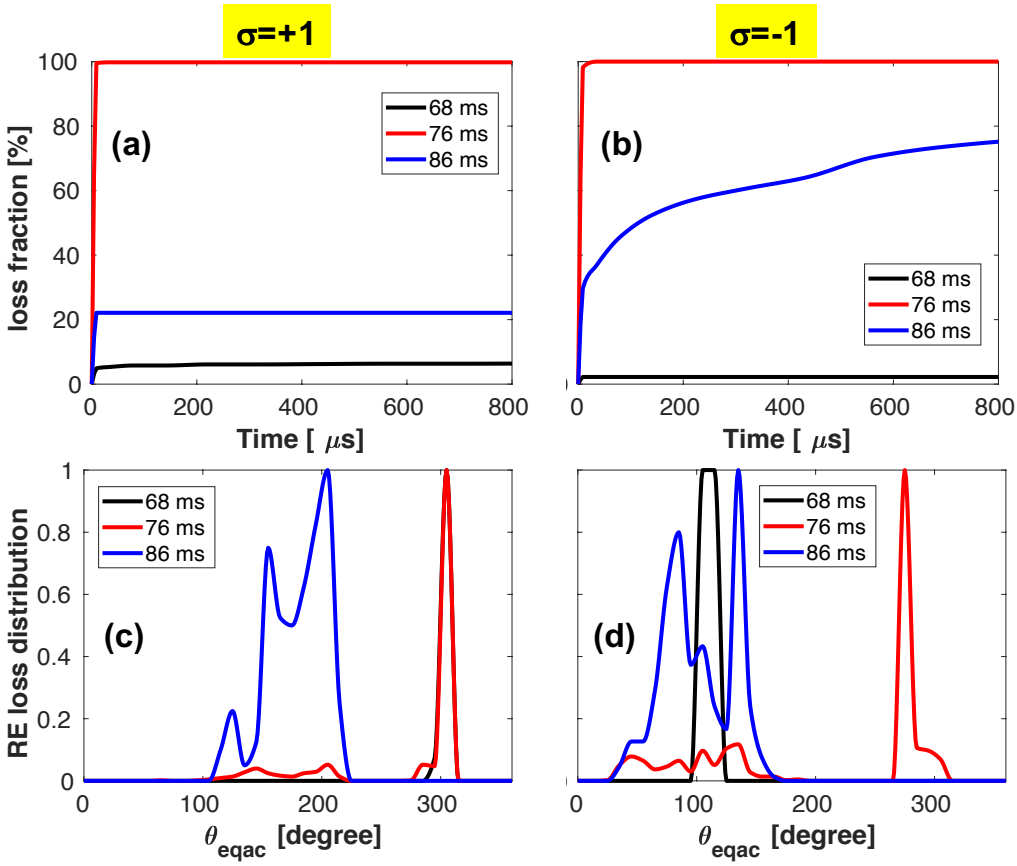

Figure 18. Comparison of (a-b) the RE loss fraction versus the simulation time, and (c-d) the final distribution of lost REs along the poloidal angle of the ITER limiting surface, for particles launched with the initial parallel velocity being in either (a,c) co- or (b,d) counter-direction to the equilibrium plasma current. In the presence are 3-D perturbations due to the $n = 1$ resistive kink instabilities in the post-disruption ITER plasmas at 68 ms (q_a below 4, left panels), 76 ms (q_a below 3, middle panels), and 86 ms (q_a below 2, right panels), respectively, with the same peak value of $|\delta B| = 18.8$ kG over the plasma volume in all cases. Considered are REs with the initial pitch angle of $\lambda_0 = 0.1$ and the particle energy of 50 MeV.

divertor with large perturbations (> 5 kG). The wetted area generally increases with the perturbation amplitude.

The above observations from Fig. 19 are also qualitatively valid for REs at lower energy levels. Figure 20 summarizes all results in terms of the RE loss fraction (a-c) and the wetted area fraction (d-f), where we vary the perturbation field from 1 kG to 18.8 kG, and the particle energy from 10 MeV to 50 MeV. Certain scatter of the results, with respect to the particle energy, are obtained for the internal kink (at 68 ms) instability. On the other hand, the RE loss properties weakly depend on the particle energy with a more global perturbation structure (at 76 and 86 ms), meaning that this kind of instability is capable of mitigating all high-energy REs in a post-disruption plasma in ITER 15 MA scenario.

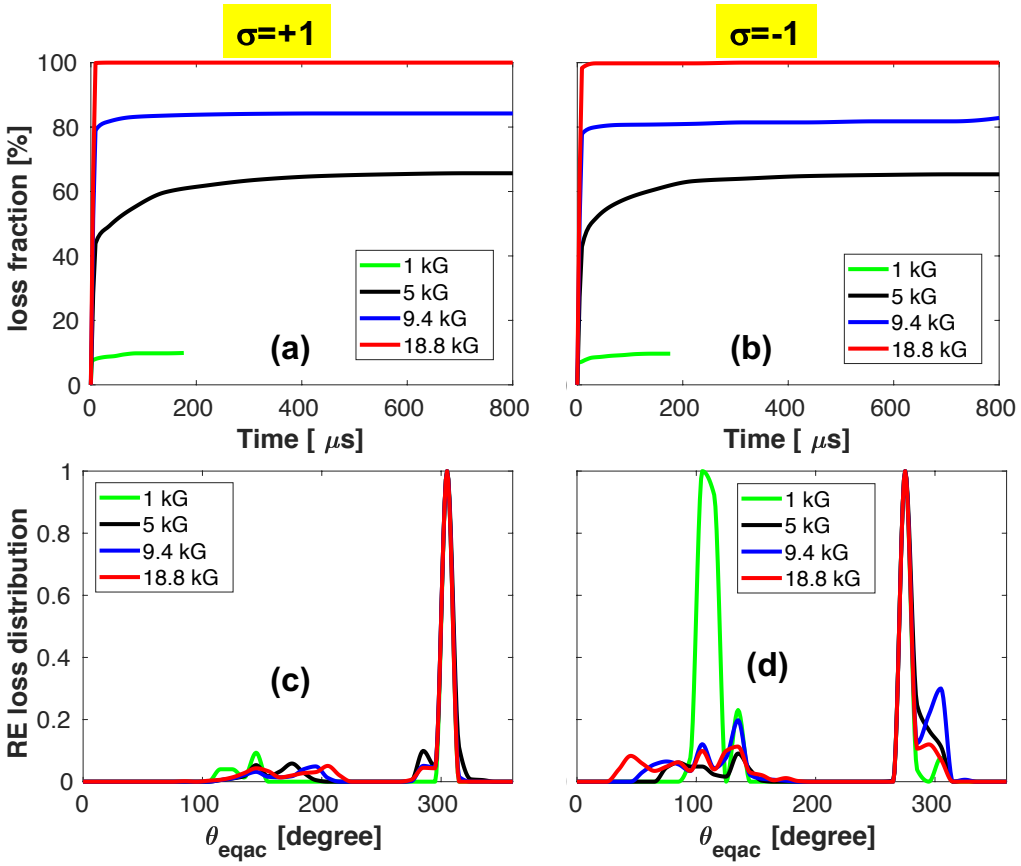

Figure 19. Comparison of (a-b) the RE loss fraction versus the simulation time, and (c-d) the final distribution of lost REs along the poloidal angle of the ITER limiting surface, for particles launched with the initial parallel velocity being in either (a,c) co- or (b,d) counter-direction to the equilibrium plasma current. In the presence are 3-D perturbations due to the $n = 1$ resistive kink instabilities in the post-disruption ITER plasma at 76 ms, with varying peak values of $|\delta B|$ over the plasma volume. Considered are REs with the initial pitch angle of $\lambda_0 = 0.1$ and the particle energy of 50 MeV.

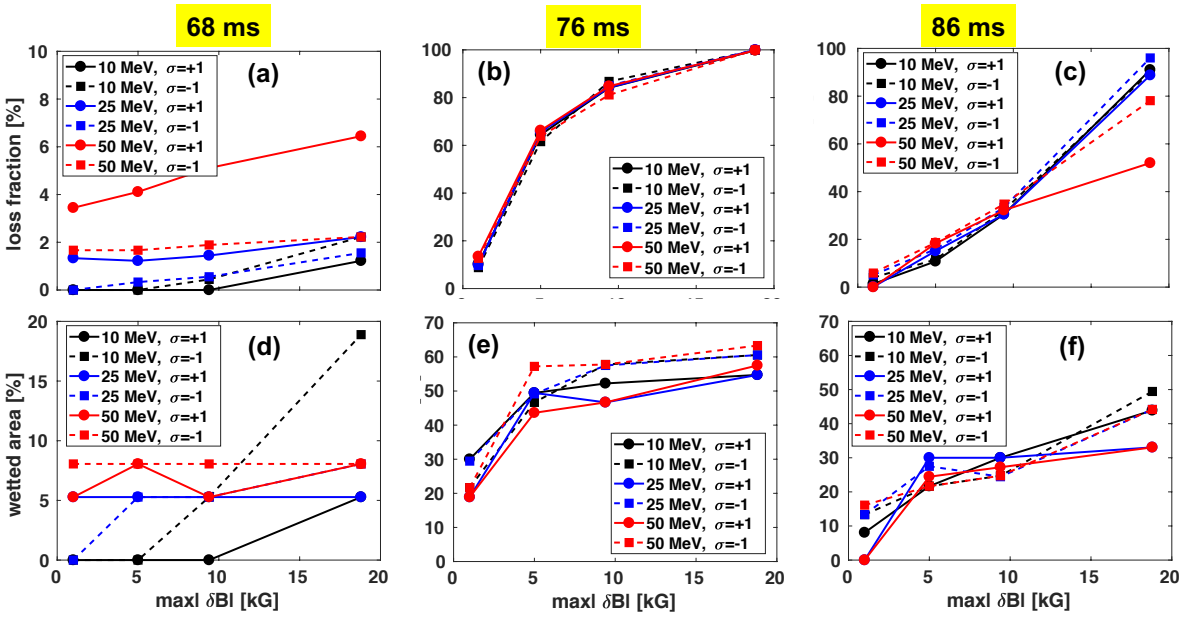

Figure 20. Comparison of (a-b) the steady state RE loss fraction, and (c-d) the wetted area fraction of the ITER limiting surface due to lost REs, while varying the peak value of $|\delta B|$ over the plasma volume and assuming different choices for the particle energy. The initial parallel velocity of REs is assumed to be either in co- ($\sigma = +1$, solid lines) or counter-direction ($\sigma = -1$, dashed lines) to the equilibrium plasma current. Considered are three post-disruption ITER equilibria at 68 ms (left panels), 76 ms (middle panels), and 86 ms (right panels), respectively, that are all unstable to the $n = 1$ resistive kink modes.

5. Conclusion and discussion

We have investigated the potential of RE mitigation by 3-D magnetic field perturbations in plasmas from the ITER 15 MA baseline D-T scenario, utilizing the MARS-F code and a drift orbit test particle tracing module (REORBIT). Two types of 3-D perturbations are considered: the $n = 3$ RMP field produced by the ELM control coils in ITER and perturbations generated by the $n = 1$ MHD instabilities in a post-disruption plasma. In the former case, the plasma response to the applied 3-D field is taken into account when tracing the RE trajectories.

The RMP field is applied to a pre-disruption plasma, mainly for the purpose of investigating the possibility of mitigating RE seeds in ITER. Modeling shows that, while the scheme appears to be somewhat effective with the vacuum field approximation - up to $\sim$40% loss fraction is possible, the predicted mitigation efficiency is substantially reduced when the plasma response is taken into account - only less than 5% loss fraction can be achieved even at 90 kAt coil current. This is due to a strong screening of the resonant magnetic field components by the plasma response, resulting in much less field line stochasticity inside the plasma. Note that even the strong plasma amplification of the perturbed field near the plasma edge, which occurs when we assume the optimal coil phasing that leads to the best ELM control in ITER, is not sufficient to enhance the RE loss here. It thus appears that other techniques (e.g. massive deuterium injection to increase the critical electric field threshold) should be considered to prevent the primary RE generation, if the goal is to control the RE seeding. On the other hand, RMP may be more effective if the RE seeds tend to be located near the plasma edge, as has been found for the hot-tail formation [48]. With the 3-D RMP field (and the pre-disruption, full-shaped plasma), the lost REs mainly hit the divertor area of the ITER limiting surface.

If it turns out to be challenging to control the RE seeding in ITER, one may have to opt for mitigating a fully developed runaway beam (after the secondary generation) by 3-D fields or by other means (e.g. impurity injection which is out of the scope of the present study). The MARS-F modeling, based on the DINA-simulated post-disruption equilibria, shows that the $n = 1$ resistive kink instabilities develop in these plasmas, as the plasma shrinks and the edge safety factor evolves and drops below integer numbers. Three post-disruption equilibria are considered here, occurring at 68, 76, and 86 ms. At 68 ms of the DINA simulation, MARS-F computes a resistive internal kink mode, when q_a drops below 4. This instability, however, is not effective in mitigating REs even at tesla-level of perturbation amplitude. As q_a drops below 3 (at 76 ms of the DINA simulation), a more global kink instability develops, that encompasses both internal and external components. This instability is capable of mitigating over 80% REs at 9.4 kG field perturbation level, and full mitigation if the perturbation amplitude is doubled. This level of perturbation, due to a strong kink instability, may be marginally achievable in ITER, given the experimental evidence from DIII-D. As q_a drops further, below 2 (at 86 ms), an external kink instability occurs, which is localized more near

the plasma edge and is therefore less efficient in mitigating REs in the considered ITER case. Nevertheless, the loss fraction is much larger than that due to the internal kink with the same overall perturbation amplitude. More importantly, the external kink instability at 86 ms can help to purge the residual REs, when the majority of them are already mitigated at 76 ms as q_a drops below 3.

An important conclusion here that we draw, is that the RE mitigation is sensitive to the eigenmode structure of the MHD instabilities. A radially global perturbation, which also occurs in DIII-D but at the time when q_a drops near 2, is the best for strong RE mitigation in post-disruption plasmas. We should point out that the plasma evolution during the VDE, and consequently the resulting MHD instabilities, is sensitive to the initial RE seed parameters (the amplitude and the profile shape) as shown in Ref. [24]. Nevertheless, occurrence of the $n = 1$ resistive kink instabilities, at low q_a values, appears to be a generic feature in post-disruption RE beam plasmas [19, 20, 24].

The wetted area on the ITER limiting surface, due to lost REs by MHD instabilities, generally increases with the perturbation amplitude (together with increasing loss fraction). At the highest perturbation level that we assume in this study (18.8 kG), the wetted area reaches ∼60% of the total limiting surface area, as q_a drops below 3. This relatively large spread of the RE strike points is a good feature for the MHD induced RE loss in ITER. The lost REs hit the outer divertor region of the limiting surface, with some fraction also hitting a wide area along the inboard side of the surface.

We remark two approximations adopted in the present study. One is the drift orbit model that we utilize, which limits our ability to trace high-energy REs (say at ~ 100 MeV). Full orbit model is needed for accurate tracing of high-energy REs. The other limitation comes from the linear MHD model, which does not predict the amplitude of the eigenfunction for the instability. Non-linear MHD (or MHD-RE hybrid) models are needed for more self-consistent simulation of the RE loss due to MHD modes in ITER post-disruption plasmas. Both of the aforementioned issues are out of our present model-code capability.

As for future work, we will investigate how a time-varying/growing perturbation affects the RE orbit loss in these post-disruption ITER plasmas. The expectation is that the effect of low-level 3D fields on the RE de-confinement will be limited, until the perturbation amplitude grows to a sufficiently high level as found in the present study. Further study is however needed in order to quantify this dynamic effect. This work assumes a simple (uniform) initial distribution of REs in the configuration space, augmented by a sensitivity study against variation of the particle energy. De-confinement of REs with large initial pitch angles is not considered here, based on the expectation that most of REs in a well-formed beam are passing particles with small pitch angle. It is, however, still useful to consider more realistic models for the initial RE distribution, in both the configuration and particle phase spaces. This will not affect the present conclusion when all particles are lost to the limiting surface due to the resistive kink instability. On the other hand, for cases where REs are partially lost, a more accurate initial distribution model should help to better quantify the loss

fraction. The combined effect of RMPs (or intrinsic 3-D fields) and MHD instabilities on the RE loss is another interesting topic of investigation. In particular, RMPs may help to increase the wetted area even when they are not capable of flushing REs from inside the plasma [49]. All the aforementioned aspects can be investigated by updating the REORBIT module, and will thus be pursued in the next work.

Acknowledgements

The work was supported by US DoE Office of Science under Contract DE-SC0016452, DE-FC02-04ER54698, DE-FG02-95ER54309. **Disclaimer:** This report was prepared as an account of work sponsored by an agency of the United States Government. Neither the United States Government nor any agency thereof, nor any of their employees, makes any warranty, express or implied, or assumes any legal liability or responsibility for the accuracy, completeness, or usefulness of any information, apparatus, product, or process disclosed, or represents that its use would not infringe privately owned rights. Reference herein to any specific commercial product, process, or service by trade name, trademark, manufacturer, or otherwise, does not necessarily constitute or imply its endorsement, recommendation, or favoring by the United States Government or any agency thereof. The views and opinions of authors expressed herein do not necessarily state or reflect those of the United States Government or any agency thereof. The work has also been carried out within the framework of the EURO-fusion Consortium. The views and opinions expressed herein do not necessarily reflect those of the European Commission. This research used resources of the National Energy Research Scientific Computing Center (NERSC), a U.S. Department of Energy Office of Science User Facility operated under Contract No. DE-AC02-05CH11231.

References

[1] Hender T.C. *et al* Progress in the ITER Physics Basis Chapter 3: MHD stability, operational limits and disruptions 2007 *Nucl. Fusion* **47** S128
[2] Rosenbluth M.N. and Putvinski S.V. 1997 *Nucl. Fusion* **37** 1355
[3] Boozer A.H. 2017 *Nucl. Fusion* **57** 056018
[4] Reux C. *et al* 2015 *J. Nucl. Mater.* **463** 143
[5] Connor J.W. and Hastie R.J. 1975 *Nucl. Fusion* **15** 415
[6] Rosenbluth M.N. *et al* 1997 *Nucl. Fusion* **37** 955
[7] Smith H.M. and Verwichte E. 2008 *Phys. Plasmas* **15** 072502
[8] Boozer A.H. 2015 *Phys. Plasmas* **22** 032504
[9] Gobbin M. *et al* 2018 *Plasma Phys. Control. Fusion* **60** 014036
[10] Zeng L. *et al* 2013 *Phys. Rev. Lett.* **110** 235003
[11] Papp G. *et al* 2011 *Plasma Phys. Control. Fusion* **53** 095004
[12] Jiang Z.H. *et al* 2016 *Nucl. Fusion* **56** 092012
[13] Mlynar J. *et al* 2019 *Plasma Phys. Control. Fusion* **61** 014010
[14] Izzo V. *et al* 2011 *Nucl. Fusion* **51** 063032
[15] Paz-Soldan C. *et al* 2019 *Plasma Phys. Control. Fusion* **61** 054001
[16] Hollmann E.M. 2015 *Phys. Plasmas* **22** 056108

[17] Paz-Soldan C. *et al* 2017 *Phys. Rev. Lett.* **118** 255002
[18] Spong D.A. *et al* 2018 *Phys. Rev. Lett.* **120** 155002
[19] Paz-Soldan C. *et al* 2019 *Nucl. Fusion* 066025
[20] Liu Y.Q. *et al* 2019 *Nucl. Fusion* **59**126021
[21] Lvovskiy A. *et al* 2020 *Nucl.Fusion* **60** 056008
[22] Fülöp T. *et al* 2008 *Phys. Plasmas* **13** 062506
[23] Aleynikov P.B. *et al* 2015 *Phys. Rev. Lett.* **114** 155001
[24] Aleynikova K. *et al* 2016 *Phys. Plasmas Rep.* **42** 486
[25] Liu C. *et al* 2018 *Phys. Rev. Lett.* **120** 265001
[26] Khayrutdinov R.R. and Lukash V.E. 1993 *J. Comput. Phys* **109** 193
[27] Lukash V.E. and Khayrutdinov R.R. 1996 *Plasma Phys. Rep.* **22** 91
[28] Liu Y.Q. *et al* 2000 *Phys. Plasmas* **7** 3681
[29] Liu Y.Q. *et al* 2010 *Phys. Plasmas* **17** 122502
[30] Liu Y.Q. *et al* 2020 *Phys. Plasmas* **27** 102507
[31] Zhang G. and del-Castillo-Negrete D. 2017 *Phys. Plasmas* **24** 092511
[32] Radhakrishnan K. and Hindmarsh A.C. 1993 *Lawrence Livermore National Laboratory Report* UCRL-ID-1138555
[33] Li L. *et al* 2019 *Nucl. Fusion* **59** 096038
[34] Gobbin M. *et al Nucl. Fusion* **61** 066037
[35] Reux C. *et al* 2021 *Phys.Review Lett.* **126** 175001
[36] Bandaru V. *et al* 2021 *Plasma Phys. Control. Fusion* **63** 035024
[37] Paz-Soldan C. *et al* "A Novel Path to Runaway Electron Mitigation via Deuterium Injection and Current-Driven MHD Instability" 2021 *Nucl. Fusion* submitted
[38] Liu Y.Q. *et al* 2011 *Nucl. Fusion* **51** 083002
[39] Liu Y.Q. *et al* 2016 *Plasma Phys. Control. Fusion* **58** 114005
[40] Carbajal L. *et al* 2017 *Phys. Plasmas* **24** 042512
[41] Somariva C. *et al* 2018 *Nucl. Fusion* **58** 016043
[42] Liu C. *et al* 2018 *Nucl. Fusion* **58** 106018
[43] Helander P. *et al* 2007 *Phys. Plasmas* **14** 122102
[44] Zhao C. *et al* 2020 *Nucl. Fusion* **60** 126017
[45] Li L. *et al* 2021 *Nucl. Fusion* **61** 096034
[46] Liu Y.Q. *et al* "Interaction between runaway electrons and internal kink in a post-disruption plasma" 2021 *Nucl. Fusion* in press
[47] Bussac M.N. *et al* 1975 *Phys. Rev. Lett.* **35** 1638
[48] Aleynikov P.B. and B.N. Breizman 2017 *Nucl. Fusion* **57** 046009
[49] Aleynikov P.B. *et al* 2010 *Proc. 37th EPS Conference on Plasma Physics* P1.1004. http://ocs.ciemat.es/EPS2010PAP/pdf/P1.1004.pdf